STUDY OF MOIRÉ MEASURING TECHNIQUES
FOR WIND TUNNEL MODEL DEFORMATION
By

ABELE & SANLORENZO

GENERAL APPLIED SCIENCE LABORATORIES, INC.
MERRICK AND STEWART AVENUES
WESTBURY, NEW YORK 11590

July 1975

Final Report for Period November 1973 to November 1974

Prepared for

ARNOLD ENGINEERING DEVELOPMENT CENTER (DY)
AIR FORCE SYSTEMS COMMAND
ARNOLD AIR FORCE STATION, TENNESSEE 37389

NOTICES

When U. S. Government drawings specifications, or other data are used for any purpose other than a definitely related Government procurement operation, the Government thereby incurs no responsibility nor any obligation whatsoever, and the fact that the Government may have formulated, furnished, or in any way supplied the said drawings, specifications, or other data, is not to be regarded by implication or otherwise, or in any manner licensing the holder or any other person or corporation, or conveying any rights or permission to manufacture, use, or sell any patented invention that may in any way be related thereto.

Qualified users may obtain copies of this report from the Defense Documentation Center.

References to named commercial products in this report are not to be considered in any sense as an endorsement of the product by the United States Air Force or the Government.

This report has been reviewed by the Information office (OI) and is releasable to the National Technical Information Service (NTIS). At NTIS, it will be available to the general public, including foreign nations.

APPROVAL STATEMENT

This technical report has been reviewed and is approved for publication.

FOR THE COMMANDER

MARSHALL K. KINGERY
Facility Development Division
Directorate of Civil Engineering

ROLAND R. GARREN
Colonel, USAF
Director of Civil Engineering

REPORT DOCUMENTATION PAGE		READ INSTRUCTIONS BEFORE COMPLETING FORM
1 REPORT NUMBER AEDC–TR–75–53	2 GOVT ACCESSION NO.	3 RECIPIENT'S CATALOG NUMBER
4 TITLE (and Subtitle) STUDY OF MOIRÉ MEASURING TECHNIQUES FOR WIND TUNNEL MODEL DEFORMATION		5. TYPE OF REPORT & PERIOD COVERED Final Report – Nov 1973 to Nov 1974
		6. PERFORMING ORG. REPORT NUMBER TR 788
7. AUTHOR(s) Manlio Abele and Ernest Sanlorenzo		8. CONTRACT OR GRANT NUMBER(s) F40600–74–C–0004
9 PERFORMING ORGANIZATION NAME AND ADDRESS General Applied Science Laboratories, Inc. Merrick and Stewart Avenues Westbury, New York 11590		10 PROGRAM ELEMENT, PROJECT, TASK AREA & WORK UNIT NUMBERS Program Element 65802F
11 CONTROLLING OFFICE NAME AND ADDRESS Arnold Engineering Development Center(DYFS) Air Force Systems Command Arnold Air Force Station, Tennessee 37389		12 REPORT DATE July 1975
		13 NUMBER OF PAGES 56
14 MONITORING AGENCY NAME & ADDRESS(if different from Controlling Office)		15 SECURITY CLASS. (of this report) UNCLASSIFIED
		15a. DECLASSIFICATION/DOWNGRADING SCHEDULE N/A

16 DISTRIBUTION STATEMENT (of this Report)

Approved for public release; distribution unlimited.

17 DISTRIBUTION STATEMENT (of the abstract entered in Block 20, if different from Report)

18 SUPPLEMENTARY NOTES

Available in DDC

19 KEY WORDS (Continue on reverse side if necessary and identify by block number)

moire effects   deformation
model tests
wind tunnels
Reynolds number

20. ABSTRACT (Continue on reverse side if necessary and identify by block number)

Moiré pattern measurement techniques for measurement of changes in the shape of aerodynamic models during wind tunnel tests was investigated. Theoretical and experimental study resulted in a recommendation of a Moiré system with a major variation. The grid is physically applied at the model surface. Images are recorded on film in two views for both the distorted and undistorted cases. These images are then processed to determine the position of the

DD FORM 1473 EDITION OF 1 NOV 65 IS OBSOLETE
1 JAN 73

20. ABSTRACT   (Continued)

grids in the undistorted condition as well as the magnitude of the
distortion suffered by the grids during the test.

AFSC
Arnold AFS Tenn

PREFACE

This final report describes the work performed by General Applied Science Laboratories, Inc. (GASL), under Contract No. F40600-74-C-0004 on an optical technique to be used in a high Reynolds number facility for model deformation measurements. The report presents first the measurements conducted at GASL using an experimental arrangement which simulates the test conditions of the facility. Based on these results the report outlines the configuration of the proposed measuring system and, in particular, the procedure for an automated processing of the experimental data.

The reproducibles used in the reproduction of this report were supplied by the authors, Manlio Abele and Ernest Sanlorenzo.

LIST OF ILLUSTRATIONS

SECTION I

INTRODUCTION

Under Contract F40600-74-C-0004 GASL has conducted a feasibility study of using a Moiré technique for measurement of aerodynamic model deformation in the high density, high Reynolds number tunnel facility (HIRT). This work consisted of a combined theoretical and experimental study of the principle of operation of several possible variations of the basic Moiré technique. The study resulted in the recommendation of a particular technique which makes use of a grid physically applied to the surface of the model at the point of interest. Images of the grid are taken with two cameras in both undistorted and distorted conditions of the surface of the model. The images are then processed to determine the position of the grids in the undistorted conditions as well as the magnitude of the distortion suffered by the grids during the test.

The actual implementation of the recommended measuring technique for the HIRT facility is the subject of the work program described in this report. Two major components are required in the measureing technique: a system of two cameras looking at the test surface through suitable windows in the inner wall of the test section and a scanning system which automatically extracts from the images of the grids affixed to the test surface the pertinent data in digital form. The output of the scanning system is then processed with standard computing software to determine the distortion of the test surface. The main problems in selecting the camera system arise from the stringent geometrical requirements of camera location, filming speed, film resolution and large number of images in each test. A filming speed close to 200 frames per second is required to collect the images of the test grid with sufficient time resolution of the test run and a high resolution film is required to generate the images of the grid with sufficient definition of the grid parameters. Commercially available films and lenses make is possible to select a 35 mm format for the cameras thereby reducing the cost and complexity which would arise in a larger format. The problem of camera format and film selection has been investigated in the current program by simulating grid dimensions and camera arrangement of the final system. Several candidate films have been tested and the images obtained with the same lens of the final system have been analyzed. The results of this part of the work is presented in Chapter 2.

Images of a test grid were systematically collected at positions and orientations simulating the different parts of the surface of a test model over the total range of specified model dimensions and pitch angles. Also at each position images were taken over the ranges of translations and rotations simulating the local distortion of the test model. The geometrical parameters of the images were measured with a microscope and correlated with the test grid position and orientation. In addition, the images were electronically scanned in a commercially available image analyzing system to determine the basic requirements of the final instrumentation. The results are presented in SECTION III

together with the set of equations which provide the distortion values from the measured image parameters.

SECTION IV of this report presents the basic configuration of the candidate instrumentation. First camera arrangement and camera selection are discussed. Second the data processing system which includes the film scanner and the image analyzer and digitizer is discussed. In particular the logic of the measuring and analyzing process is presented with the basic requirements of the operational system. Finally, the conclusions and recommendations for a possible improvement of the measuring precision are presented.

SECTION II

DATA RECORDING SYSTEM

2.1 INTRODUCTION

The feasibility study described in Reference (1) resulted in the recommenda-
tion of a data recording system illustrated by the schematic of Figure (1).
Two movie cameras, C, C' , are mounted outside of the test section with a
90° angle between the two optical axes. The test surface S is located
within the field of view of the two cameras. The measuring technique requires
a grid or a distribution of grids built into the surface of the model. Images
of the grids are taken with the two cameras in both situations of undistorted
and distorted test surface to provide the data required for the computation of
the local distortion.

This section presents the work performed in the simulation of the arrangement
of Figure (1) and the results obtained in the optical measurement of the geo-
metrical parameters of the grid images.

2.2 TEST GRIDS

Rather than building a wing-like structure to simulate a typical test surface
it was decided to build an element of test surface with the dimensions of a
grid and to mount it on a supporting structure where both translational and
rotational degrees of freedom can be independently controlled. This arrange-
ment has the advantage of providing a maximum flexibility in covering the
entire range of specified geometrical parameters and simplifies the problem
of a direct measurement of position and orientation of the test grid.

Based on the results presented in Reference (1) a line grid was selected with
a 1 mm period and a one-to-one ratio of line width and spacing. A length of
150 mm was selected for the grid with a resulting total number of lines of 150.
The width of the grid has no bearing on the measurements and was arbitrarily
selected at 10 mm (3/4 inches).
19

To accommodate this grid the element of test surface was built with a rectangular
aluminum block 190 mm long and 19 mm wide. The lines of the grid were built
first by machining rectangular grooves .5 mm wide and .3 mm deep into the sur-
face of the aluminum block. Subsequently the grooves were filled with a dark
grey epoxy and the block was machined again to obtain a uniform plane surface
with no discontinuity between epoxy and metal. A picture of such a grid is
shown in Figure (2).

Three identical line grids were built, one to be used as the test element of
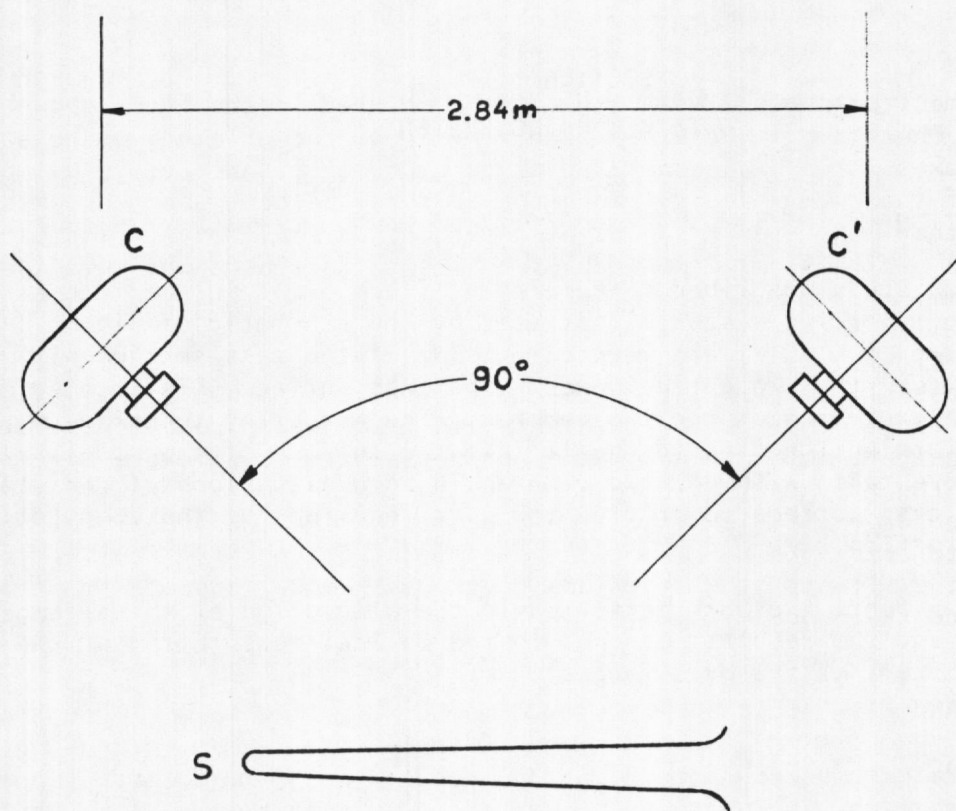surface, and the other two provide the reference points in the experimental setup.

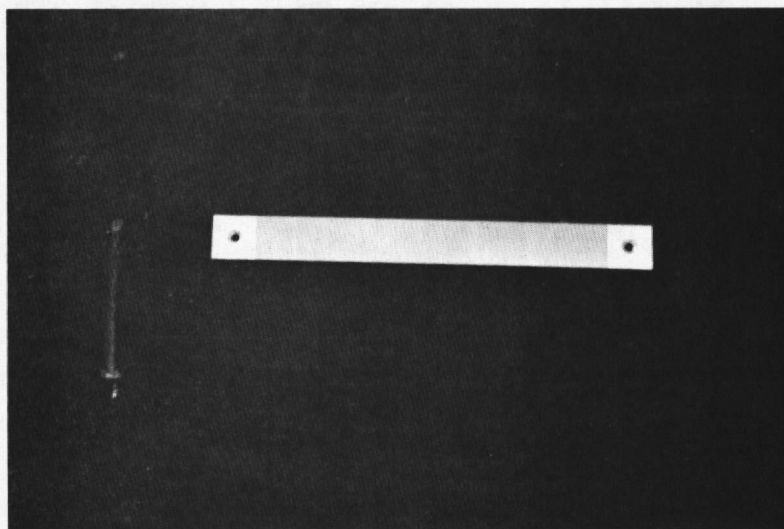FIGURE 1. SCHEMATIC OF THE DATA RECORDING SYSTEM

FIGURE 2. ELEMENT OF TEST SURFACE WITH THE LINE GRID

8

The test element of surface with the grid is mounted in the frame shown in Figure (3). The frame is built in such a way that the grid can be rotated about three axes which are perpendicular to each other and have in common the center of the grid. In addition, the grid can be bent about an axis parallel to the lines over a radius of curvature as small as 1 m and can be translated in a direction perpendicular to its surface by a maximum displacement of 100 mm.

The frame of Figure (3) is attached to the support shown in Figure (4) which allows the possibility of rotating the test grid about a horizontal axis to simulate the range of pitch angles. The grid frame can also be translated both along the vertical column and the horizontal arm to simulate different positions of the grid on the surface of the test model over dimensions of 90 cm. One observes in Figure (4) the supports of the two additional grids which simulate reference points of the test model in the HIRT facility required to separate the effects of distortions of the test model support from the distortion of the test model itself.

2.3 CAMERA AND FILM SELECTION

Several laboratory medium speed movie cameras in the 35 mm format are commercially available and can be readily adapted to this particular application. These cameras can provide the required frame rate with electronically controlled electric drive and precision film transport and frame registration. Typical characteristics are a frame rate of 180 fps with an accuracy of $\pm 1\%$ and film capacity from 200 ft to 1000 ft with interchangeable magazines. With a 2.5 secs run time the 200 ft magazine should be more than adequate and a camera body is available which occupies a small volume 12.5 inches long with a 5.5 x 5.5 inches square cross section. Two such cameras would be installed in the facility according to the schematic of Figure (1).

The distance of the film plane of each camera from the center of the test section would be approximately 2 m. Hence a wide angular lens is required to bring within the field of view of each camera test models having dimensions of the order of 90 cm. In addition, the lens must have high resolution to provide sharp images of the grids affixed to the surface of the model. A lens having the required characteristics is the Schneider Kreuznack Xenon 1:2/35 mm motion picture camera and can resolve approximately 600 lines per millimeter. This lens would then be used in the actual instrumentation of the facility and consequently was selected also for the current program. However, as far as the camera is concerned, for convenience it was decided to use a still camera, rather than a motion picture camera to take the images of the line grid described in SECTION II-2. A Contax 35 mm still camera was selected and an adapter was built to use it with the Xenon 1:2/35 lens. Figure (5) shows the camera with the Xenon lens mounted on its support. To simulate the two camera arrangement of the final measuring system, two columns have been rigidly attached to the
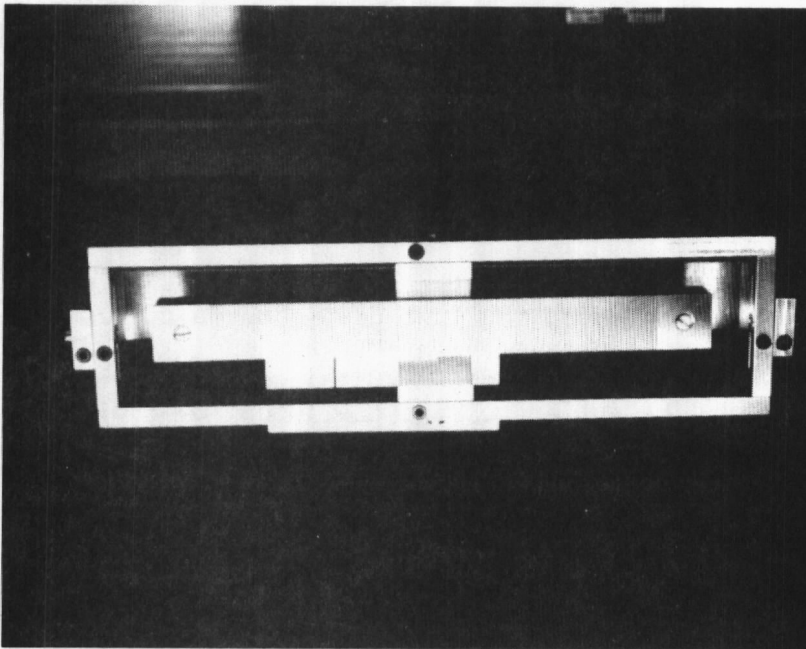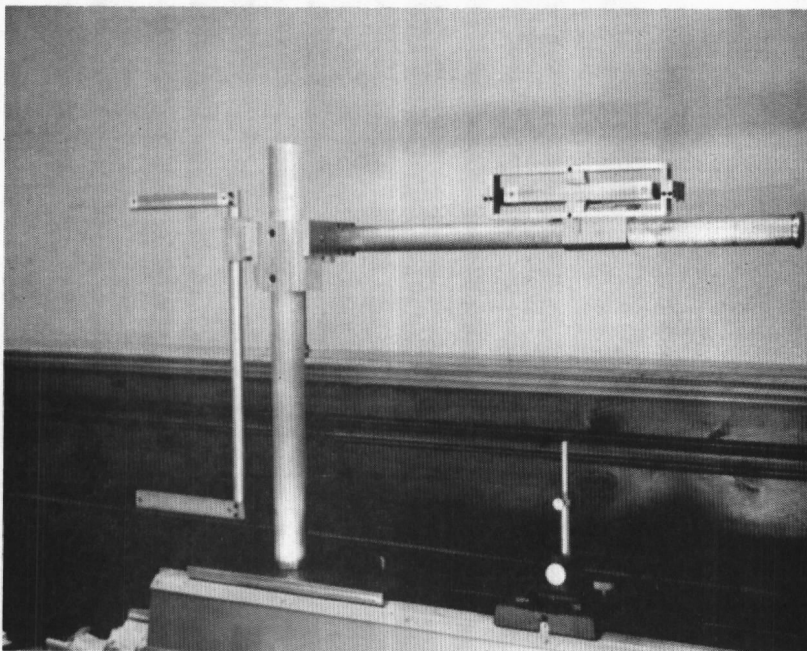
FIGURE 3. FRAME OF THE TEST SURFACE

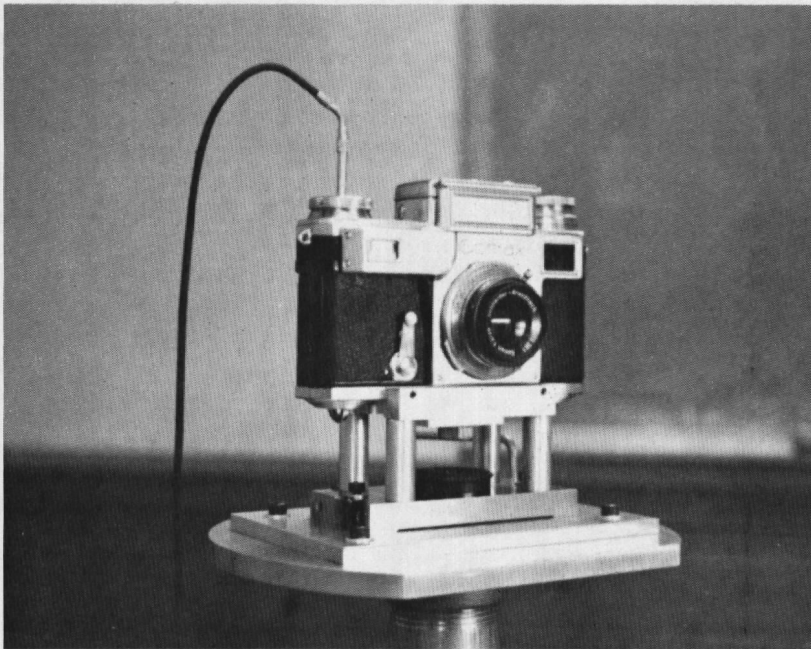FIGURE 4. SUPPORT OF THE TEST SURFACE

FIGURE 5. CAMERA AND ITS SUPPORT

floor at a distance of 286 cm from each other. Two horizontal platforms have been mounted on the two columns. As shown in Figure (5) the camera is attached to a precision hardened steel rectangular base whose position on each platform is fixed by a set of three centering pins to insure the correct orientation of the camera in the two positions defined by the schematic of Figure (1). Thus the two camera arrangement of the final system was simulated by moving the same camera from one column to the other. The intersection of the two optical axes corresponds to the center of the test section.

The use of Xenon lens made it necessary to recalibrate the camera focussing. The setting was then adjusted for optimum focusing with an object located at the intersection of the two optical axes. This same setting was maintained for the entire program of photographic data collection.

Preliminary tests were conducted with the camera to select a suitable film. This particular application requires a high resolution film and a reasonable speed to be compatible with the required movie camera frame rate and a practical intensity of illumination of the test model. The initial series of photographic data was taken with Kodak Panatomic-X film (ASA 32) and Kodak 2496 RAR film (ASA 125). Both are black and white films with a resolving power of 125 lines/mm. The images obtained with these films are adequate for the laboratory optical measurement of the geometrical parameters of the test grid. However, the processing of the images in an automated scanner described in a following section gave unsatisfactory results, since the film resolution proved marginal for the required accuracy of the scanning process. Commercially available films with resolving power much higher than either the Panatomic-X or the 2496 RAR film could not be used because their speed is too low for the present application. A satisfactory compromise was found in the Kodak Recordak AHU Microfilm 5460 which is a high contrast film with a resolving power of 630 lines/mm. The high contrast characteristic is not a serious limitation for this particular application where the film has to satisfy only to the requirement of separating the grid lines from the background of the metallic surface. Obviously, the speed of the Recordak Microfilm is lower than the Panatomic-X. In preliminary tests with the images of the grid built into the aluminum block of Figure (2) the equivalent ASA number turned out to be approximately 15, which is still consistent with a practical illumination system of the model in the test section of the facility.

Another advantage of the Recordak Microfilm is that it is specifically designed for an automated rapid developing process. With Prostar Developer, the developing time ranges from 10 to 15 secs. What would be an advantage in the final system posed a problem in the work done with the still camera where each roll of film had to be manually developed and a series of tests were required to achieve a much longer developing time. The best results were obtained with D11 developer diluted with water in a 1:1 ratio at 70° F. In these conditions the optimum developing time was found to be 4 minutes. The Recordak AHU Microfilm 5460 was then selected for the collection of the experimental data with the test grid described in SECTION II-2. A typical sequence of frames showing the image of a test grid is presented in Figure (6).
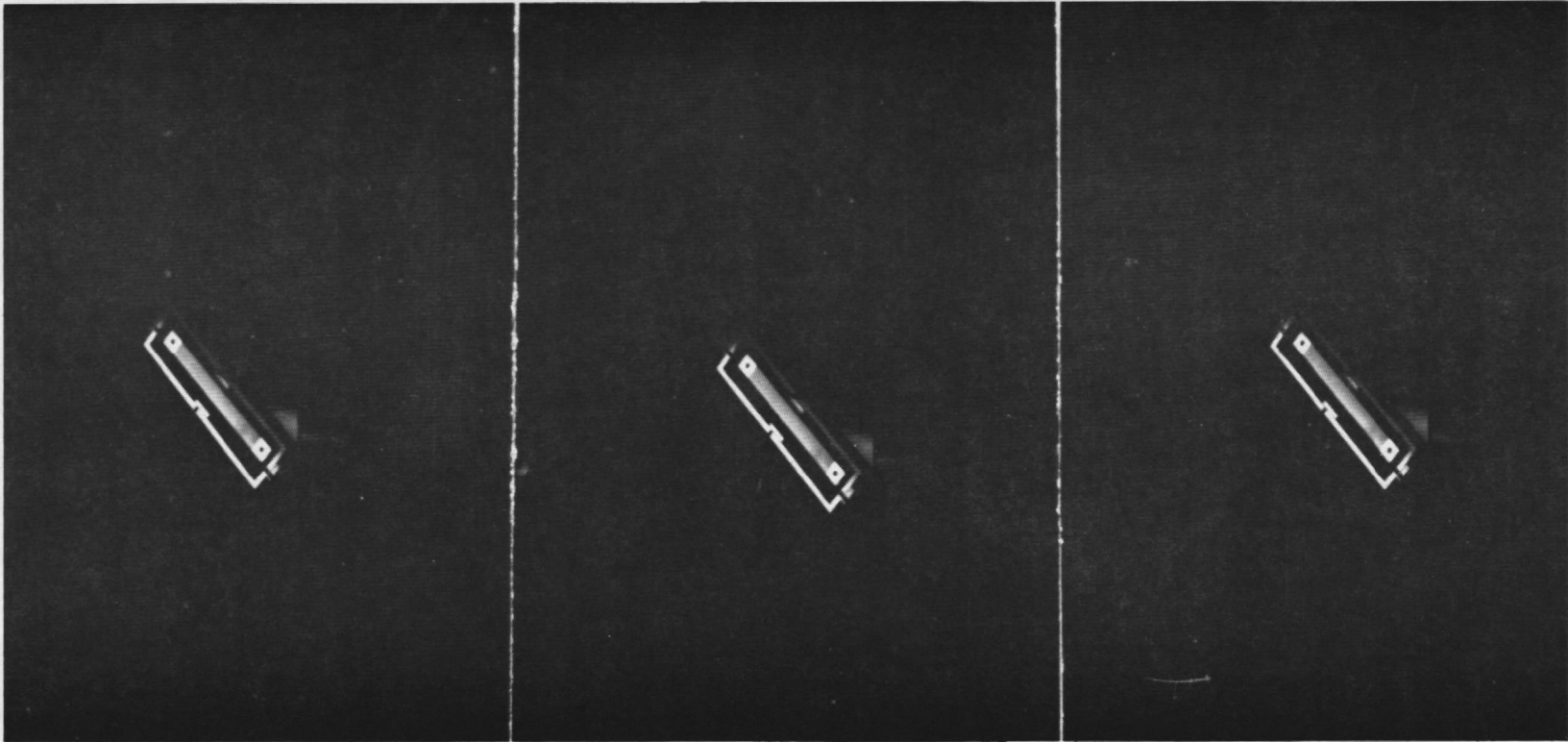
FIGURE 6. SEQUENCE OF IMAGES OF THE TEST GRID

SECTION III

CORRELATION OF MEASUREMENT OF GRID
POSITION AND IMAGE PARAMETERS

3.1 INTRODUCTION

Once the pictures of a test grid are obtained with the two camera arrangement
discussed in the previous section, the data reduction process begins in order
to extract from the images of the grid the distortion of the test surface.
As described in Reference (1) the data reduction process would be developed
in two steps: first the images of the grid obtained from the two cameras prior
to the test are processed in order to determine the position of the grid in
the undistorted condition; and second, the images of the grid obtained with
one camera in both distorted and undistorted conditions are correlated to
each other in order to determine the magnitude of the distortion during the
test.   This procedure is more precise than the method of obtaining the dis-
tortion from the two independent measurements of the grid portion prior and
during the test.

When the two images of the grid obtained with the same camera (in both dis-
torted and undistorted conditions) are superimposed to each other a Moiré
or interference pattern is generated and this pattern can be correlated to
the grid distortion provided that the original position of the grid is known.
Reference (1) has shown how a nulling technique can be used in the analysis
of the interference pattern in order to extract the required information.

This section defines the set of geometrical parameters which must be extracted
from the images obtained in two cameras in order to compute both position and
distortion of the test grid.   These parameters and the frame of reference of
the test grid have been selected according to what appears to be the most
convenient approach from the point of view of an automatic scanning and
digitizing process.   Also the governing equations which correlate the images
with the grid position are presented in SECTIONS II-2 and III-3.   In SECTION
III-4 the correlation between the test grid distortion and the changes of
the parameters of the grid images is presented.   In SECTION III-5 the
measurements of the relevant parameters of the grid images obtained with the
camera arrangement of SECTION I are presented and computed values of the grid
distortion are compared with the direct measurements.

3.2 CORRELATION OF THE GRID IMAGES OF THE TWO CAMERAS WITH THE TEST GRID

In the final arrangement of HIRT facility instrumentation two identical cameras
would be used to record the images of the grid affixed to the test surface in
order to obtain the grid positions in the undistorted model conditions.

The optical axes of the two cameras would be in the same plane at a 90°
angle with respect to each other.

As shown in Figure (7) assume a frame of reference x, y, z with the axes
x, z coinciding with the optical axes of the cameras. Points C_1, C_2 in
Figure (7) represent the center of the iris diaphragms of the two cameras
and v is the distance of C_1, C_2 from the planes of the respective images.
Assume also that C_1, C_2 are located at the same distance from the
origin O_r of the system x, y, z and let u denote that distance.

Let P_o be the center of a test grid and P_{i1}, P_{i2} its images in the two
cameras. The positions of the grid images are defined by the following
parameters;

x_{i1}, y_{i1} coordinates of P_{i1} in the first camera

y_{i2}, z_{i2} coordinates of P_{i2} in the second camera

α_1 angle of the principal axis of the grid
                       image in the first camera with respect
                       to the axis x

α_2 angle of the principal axis of the grid
                       image in the second camera with respect
                       to the axis z

The principal axes of the two grid images are denoted by $\bar{x}$ in the first
camera and $\bar{z}$ in the second camera. In addition to the aforementioned
parameters, denote by $\lambda(\bar{x})$ the period of the intersection of the grid
image lines with the axis $\bar{x}$ as a function of $\bar{x}$ in the firest camera as
shown in Figure (8). An identical function could be defined for the
image of the grid in the second camera, but it is not going to be used
in the correlation analysis. The coordinates of P_o are related to the
coordinates x_{i1}, y_{i1} and y_{i2}, z_{i2} of the two images by the elementary
equations
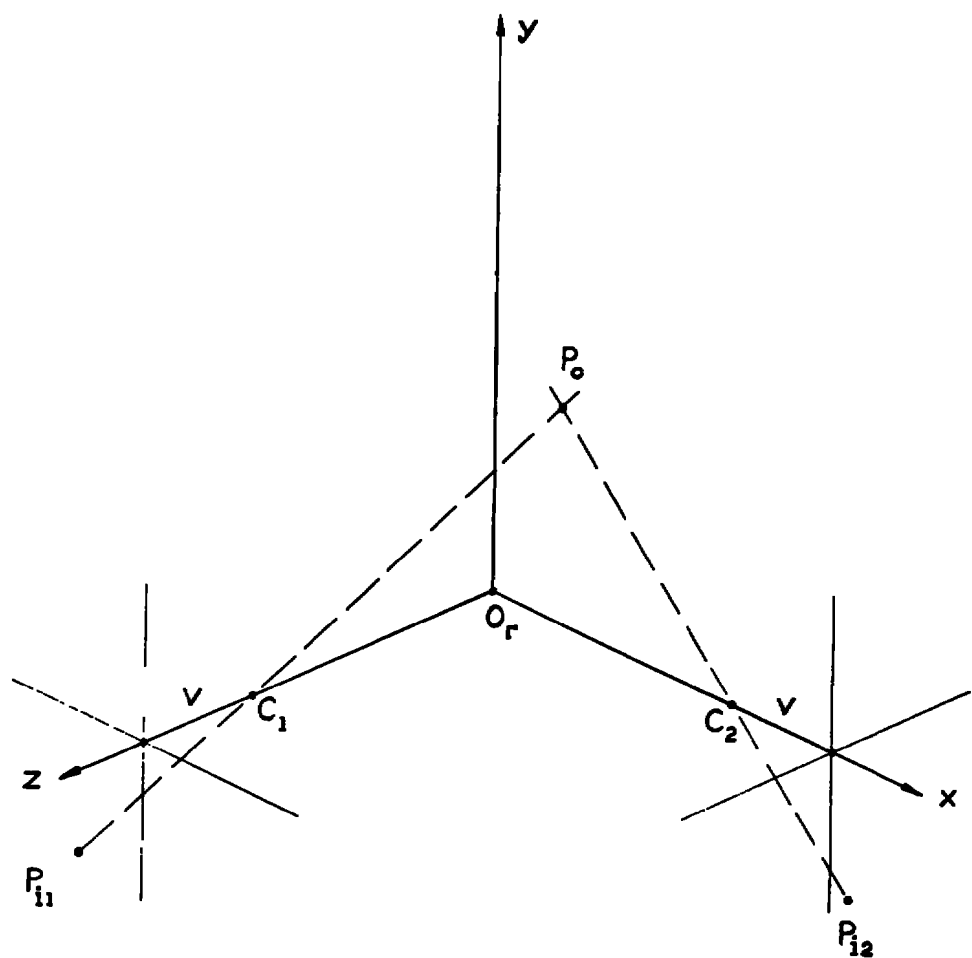
FIGURE 7. FRAME OF REFERENCE OF THE TWO CAMERAS
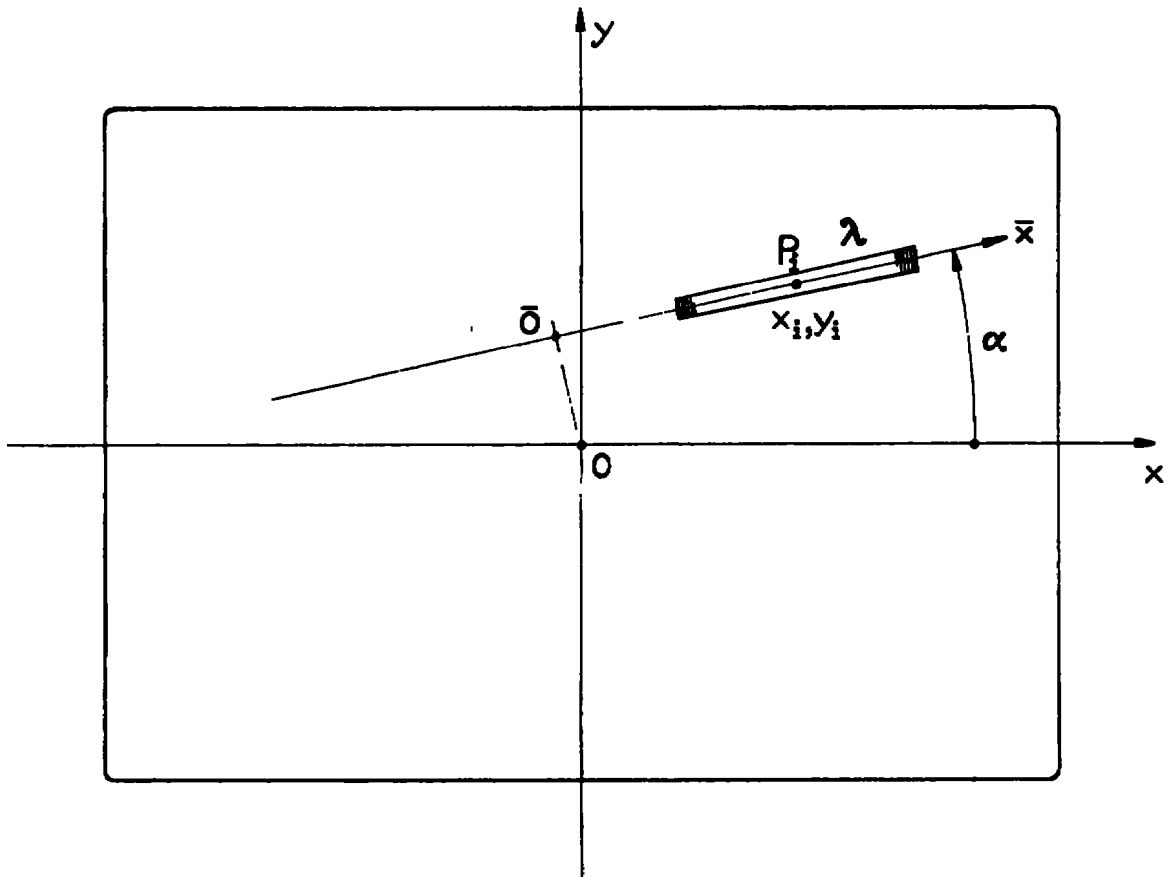
FIGURE 8. REFERENCE SYSTEM OF THE IMAGE OF THE TEST GRID

where did this come from?

is this mag factor?

$$x = \frac{u}{v} \cdot \frac{1 - \dfrac{z_{i2}}{v}}{1 - \dfrac{x_{i1}\, z_{i2}}{v^2}} \, x_{i1}$$

$$y = \frac{u}{v} \cdot \frac{1 - \dfrac{z_{i2}}{v}}{1 - \dfrac{x_{i1}\, z_{i2}}{v^2}} \, y_{i1}$$

$$z = \frac{u}{v} \cdot \frac{1 - \dfrac{x_{i1}}{v}}{1 - \dfrac{x_{i1}\, z_{i2}}{v^2}}$$

(1)

In addition to the coordinates x, y, z of P_0 , two angular coordinates are required to define the orientation of the principal axis of the test grid in the frame of reference x, y, z. It is convenient to select these angular coordinates as in a system of spherical coordinates:

ϕ angle between the grid principal axis and the axis z

θ angle between the axis x and the projection of the principal axis of the grid on the plane z = 0

Assume that the length of the test grid is L and denote by L_x , L_y , L_z the projections of L on the axis x, y, z respectively. L_x , L_y , L_z are determined by two systems of equations identical to (1) from the measured coordinates of the end points of the grid images in the two cameras. Then the angles ϕ and θ are given by

$$\cos \phi = \frac{L_z}{L} \quad ; \quad \cos \theta = \frac{L_x}{L \sin \phi}$$

(2)

18

3.3 CORRELATION OF ONE GRID IMAGE WITH THE TEST GRID POSITION

Consider only one of the two images of the same grid, for instance the image obtained with the first camera. Figure (8) schematically shows one frame of the film with the image of the grid. For simplicity, in the following analysis, the subscript i is dropped from the parameters of the image of the grid. The point P_i in Figure (8) which represents the image of the center P_o of the test grid, is the center point of the centerline of the grid image. Both the test grid and the grid image are schematically represented in Figure (9) by the segments of straight lines L and L_i respectively. The principal axis $\underline{x}$ of the grid image is the interception of the plane of the image $z = 0$ with the plane formed by the test grid and its image. The angle β between these two planes is given by

$$\tan \beta = \frac{1}{v} \ (y_i \ \cos \alpha - x_i \ \sin \alpha) \tag{3}$$

In the plane formed by the test grid and its image, select a system of coordinates ξ, η with the axis η parallel to the plane $z = 0$ and the origin coincident with the center C of the iris diaphragm of the camera as shown in Figure (9). Denote by ξ_o, η_o the coordinates of the center point P_o of the test grid and by γ the angle between the grid axis and the η axis.

In the system of reference ξ, η the coordinates of point P_i of the grid image are

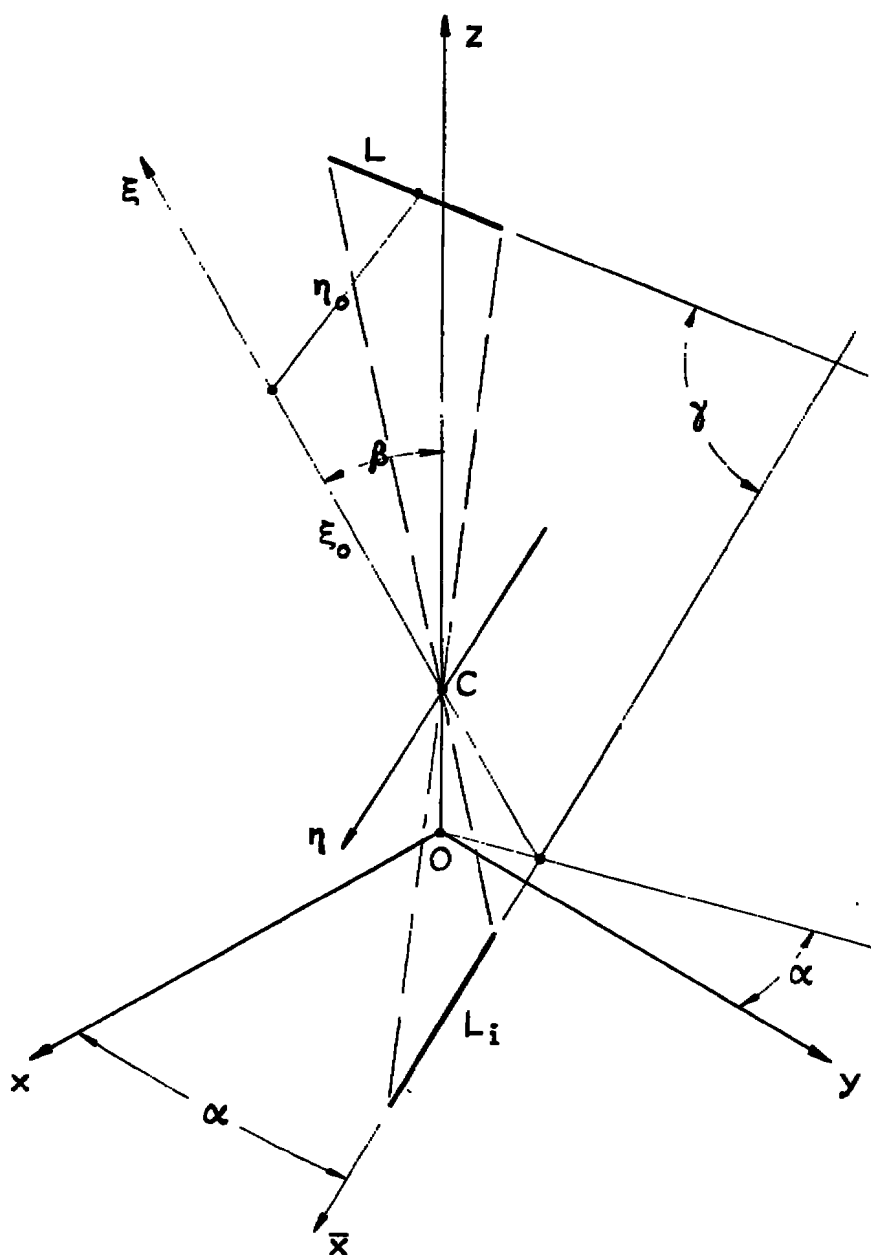$$\xi_i = - \frac{v}{\cos \beta} \ ; \quad \eta_i = x_i \ \cos \alpha + y_i \ \sin \alpha \tag{4}$$

FIGURE 9. REFERENCE SYSTEM OF TEST GRID AND GRID IMAGE

The equations relating ξ_o^-, η_o, γ to the parameters of the grid image are

$$\tan\gamma = -\xi_i \; \frac{\left(\frac{1}{2\lambda} \; \frac{d\lambda}{d\bar{x}}\right)_i}{1 - \eta_i \left(\frac{1}{2\lambda} \; \frac{d\lambda}{d\bar{x}}\right)_i}$$

$$\xi_o = \frac{\lambda_o}{\lambda_i} \; (-\xi_i \cos\gamma + \eta_i \sin\gamma) \tag{5}$$

$$\eta_o = -\frac{\eta_i}{v} \; \xi_o \cos\beta$$

where λ_i and $(d\lambda/d\bar{x})_i$ are the values of the period λ of the grid image lines and its derivative respectively at P_i. Once the values of ξ_o, η_o, λ are obtained, the position of the test grid in the original frame of reference x,y,z is readily evaluated. The coordinates x_o, y_o, z_o of P_o are

$$x_o = \xi_o \sin\alpha \sin\beta - \eta_o \cos\alpha$$

$$y_o = -\xi_o \cos\alpha \sin\beta - \eta_o \sin\alpha \tag{6}$$

$$z_o = \xi_o \cos\beta + v$$

From γ and β it is then possible to compute the angular coordinates ϕ and θ which give the orientation of the test grid in the frame of reference x,y,z as defined in the previous section.

One has

$$\cos\phi = \cos\beta \; \sin\gamma$$

$$\theta = \frac{\pi}{2} - \alpha + \psi \tag{7}$$

where

$$\cos\psi = \frac{\sin\beta \ \sin\gamma}{\sqrt{1 - \cos^2\beta \ \sin^2\gamma}} \qquad (8)$$

Systems 6 and 7 are the equations which determine position and orientation of the test grid.

Then, in principle, the analysis of either of the two images would be sufficient to determine position and orientation of the test grid. The three coordinates of the grid center point P_o and the two angular coordinates of the grid axis are obtained from the measurement of the five parameters x_i, y_i, α, λ_i and $(d\lambda/d\bar{x})_i$. The basic advantage of the two camera approach is that the measurements of center point position is independent of the measurement of the grid orientation. Furthermore, a higher precision is achieved in the measurement of the center point position because it is not dependent upon the measurement of the gradient of the period λ_i of the grid image.

The dependence of λ_i and $(d\lambda/d\bar{x})_i$ upon the coordinates of the grid in the plane ξ,η is expressed by the following equations

$$\frac{\partial\lambda_i}{\partial\gamma} = - \lambda_i \ \frac{\xi_o \ \sin\gamma + \eta_o \ \cos\gamma}{\xi_o \ \cos\gamma - \eta_o \ \sin\gamma}$$

$$\frac{\partial\lambda_i}{\partial\xi_o} = - \frac{\lambda_i}{\xi_o} \ \frac{\xi_o \ \cos\gamma - 2\eta_o \ \sin\gamma}{\xi_o \ \cos\gamma - \eta_o \ \sin\gamma} \qquad (9)$$

$$\frac{\partial\lambda_i}{\partial\eta_o} = - \lambda_i \ \frac{\sin\gamma}{\xi_o \ \cos\gamma - \eta_o \ \sin\gamma}$$

and

$$\frac{\partial}{\partial \gamma} \left(\frac{d\lambda}{d\bar{x}}\right)_i = 2 \frac{\lambda_o}{\xi_o} \cos\gamma$$

$$\frac{\partial}{\partial \xi_o} \left(\frac{d\lambda}{d\bar{x}}\right)_i = -\frac{1}{\xi_o} \left(\frac{d\lambda}{d\bar{x}}\right)_i \qquad (10)$$

$$\frac{\partial}{\partial \eta_o} \left(\frac{d\lambda}{d\bar{x}}\right)_i = 0$$

3.4   CORRELATION OF GRID IMAGES WITH TEST GRID DISTORTION

Assume now a distortion of the test surface resulting in a change of the grid image defined by the change

$$\delta x_i, \quad \delta y_i, \quad \delta\alpha, \quad \delta\lambda_i, \quad \delta\left(\frac{d\lambda}{d\bar{x}}\right)_i \qquad (11)$$

of the parameters x_i, y_i, α, λ_i and $(d\lambda/d\bar{x})_i$. Within the limits of small distortions, where the linear approximation is valid, the angle β suffers a change

$$\delta\beta = -\frac{\cos^2\beta}{v} \left[\sin\alpha \, \delta x_i - \cos\alpha \, \delta y_i + \eta_i \, \delta\alpha\right] \qquad (12)$$

and the coordinates ξ_i, η_i change by

$$\delta\xi_i = \sin\beta \left[\sin\alpha \, \delta x_i - \cos\alpha \, \delta y_i + \eta_i \, \delta\alpha\right]$$

$$\qquad (13)$$

$$\delta\eta_1 = \cos\alpha \, \delta x_i + \sin\alpha \, \delta y_i + v\tan\beta \, \delta\alpha$$

Thus in the new plane $\xi_i + \delta\xi_i$, $\eta_i + \delta\eta_i$, the orientation of the test grid is given by the angle $\gamma + \delta\gamma$ where

$$\delta\gamma = \frac{1}{2\xi_i} \sin 2\gamma \ \delta\xi_i - \frac{1}{\xi_i} \sin^2\gamma \ \delta\eta_i$$

$$- \frac{1}{2} \sin 2\gamma \left[1 - \frac{\eta_i}{\xi_i} \tan\gamma\right] \frac{\delta\lambda_i}{\lambda_i} \tag{14}$$

$$+ \frac{1}{2} \sin 2\gamma \left[1 - \frac{\eta_i}{\xi_i} \tan\gamma\right] \left(\frac{d\lambda}{dx}\right)_i^{-1} \ \delta\left(\frac{d\lambda}{dx}\right)_i$$

and the change in position of the grid center is given by

$$\delta\xi_o = - \frac{\lambda_o}{\lambda_i} \cos^3\gamma \left[1 - \frac{\eta_i}{\xi_i} \tan\gamma\right] \delta\xi_i$$

$$+ \frac{\lambda_o}{\lambda_i} \sin\gamma \cos^2\gamma \left[1 - \frac{\eta_i}{\xi_i} \tan\gamma\right] \ \delta\eta_i$$

$$\tag{15}$$

$$- \left[\xi_o + \frac{1}{2} \frac{\lambda_o}{\lambda_i} \sin 2\gamma \ (1 - \frac{\eta_i}{\xi_i} \tan\gamma) \ (\xi_i \sin\gamma + \eta_i \cos\gamma)\right] \frac{\delta\lambda_i}{\lambda_i}$$

$$+ \frac{1}{2} \frac{\lambda_o}{\lambda_i} \sin 2\gamma \ (1 - \frac{\eta_i}{\xi_i} \tan\gamma) \ (\xi_i \sin\gamma + \eta_i \cos\gamma) \left(\frac{d\lambda}{dx}\right)_i^{-1} \delta\left(\frac{d\lambda}{dx}\right)_i$$

and

$$\delta\eta_o = - \eta_o \left[\frac{1}{\xi_i} + \frac{\lambda_o}{\lambda_i\xi_o} \cos 3\gamma \ (1 - \frac{\eta_i}{\xi_i} \tan\gamma)\right] \ \delta\xi_1$$

$$+ \eta_o \left[\frac{1}{\eta_i} + \frac{\lambda_o}{\lambda_i\xi_o} \sin\gamma \cos^2\gamma \ (1 - \frac{\eta_i}{\xi_i} \tan\gamma)\right] \ \delta\eta_i$$

$$\tag{16}$$

$$- \frac{\eta_o}{\xi_o} \left[\xi_o + \frac{1}{2} \frac{\lambda_o}{\lambda_i} \sin 2\gamma \ (1 - \frac{\eta_i}{\xi_i} \tan\gamma) \ (\xi_i \sin\gamma + \eta_i \cos\gamma)\right] \frac{\delta\lambda_i}{\lambda_i}$$

$$+ \frac{1}{2} \frac{\lambda_o}{\lambda_i} \frac{\eta_o}{\xi_o} \sin 2\gamma \ (1 - \frac{\eta_i}{\xi_i} \tan\gamma) \ (\xi_i \sin\gamma + \eta_i \cos\gamma) \left(\frac{d\lambda}{dx}\right)_i^{-1} \delta\left(\frac{d\lambda}{dx}\right)_i^{-1}$$

By means of Equations (13), (14), (15), (16) and by differentiation of Equations (6) and (7) translation and rotation of the test grid can be written in the original frame of reference x, y, z.

3.5 ANALYSIS OF THE PHOTOGRAPHIC DATA

The 150 lines, 1 mm period, grid described in SECTION II-2 was used for the experimental evaluation of the measuring process. The 35 mm still camera equipped with the Schneider Krenznach Xenon lens was used to photograph the test grid with the AHU Microfilm 5460. To simulate the two camera arrangements of the final system the 35 mm camera was positioned on the platforms of the two columns described in SECTION II-3, which are located at a distance of 284 cm apart from each other. The optical axes in the two positions are positioned in the same horizontal plane at an angle of 90° with respect to each other. A systematic program of collection of photographic data was developed with test grid positions and orientations which simulate the specified range of test surface dimensions and positions in the test section of the HIRT facility. With the support of the test grid oriented as shown in Figure (4) the camera arrangement used in the collection of the photographic data simulates a final configuration with the two cameras located in a plane perpendicular to the axis of the test section.

Upon development of the film, the grid images were analyzed and measured with an industrial microscope equipped with a cross-traveling high precision micrometer stage. The two micrometers of the stage in the x and y directions allows a direct reading of the frame position within 2μ over a total travel of 50 mm.

As required by the correlation procedure described in the previous sections, the parameters x_i, α and λ were measured in each grid image. In particular, the value of λ at each point of the axis $\bar{x}$ was taken as the average of the spacing between ten lines of the grid image measured around that point along $\bar{x}$.

As an example consider one of the images of Figure (6). Figure (10) represents the plotting of $\lambda(\bar{x})$ of the grid image versus $\bar{x}$. The coordinates x_i, y_i, of the center point of the centerline are

$$x_i = 2.410 \text{ mm} \quad ; \quad y_i = -.152 \text{ mm}$$

and the angle between the grid image axis and the axis x is

$$\alpha = 1° \, 30'$$

25
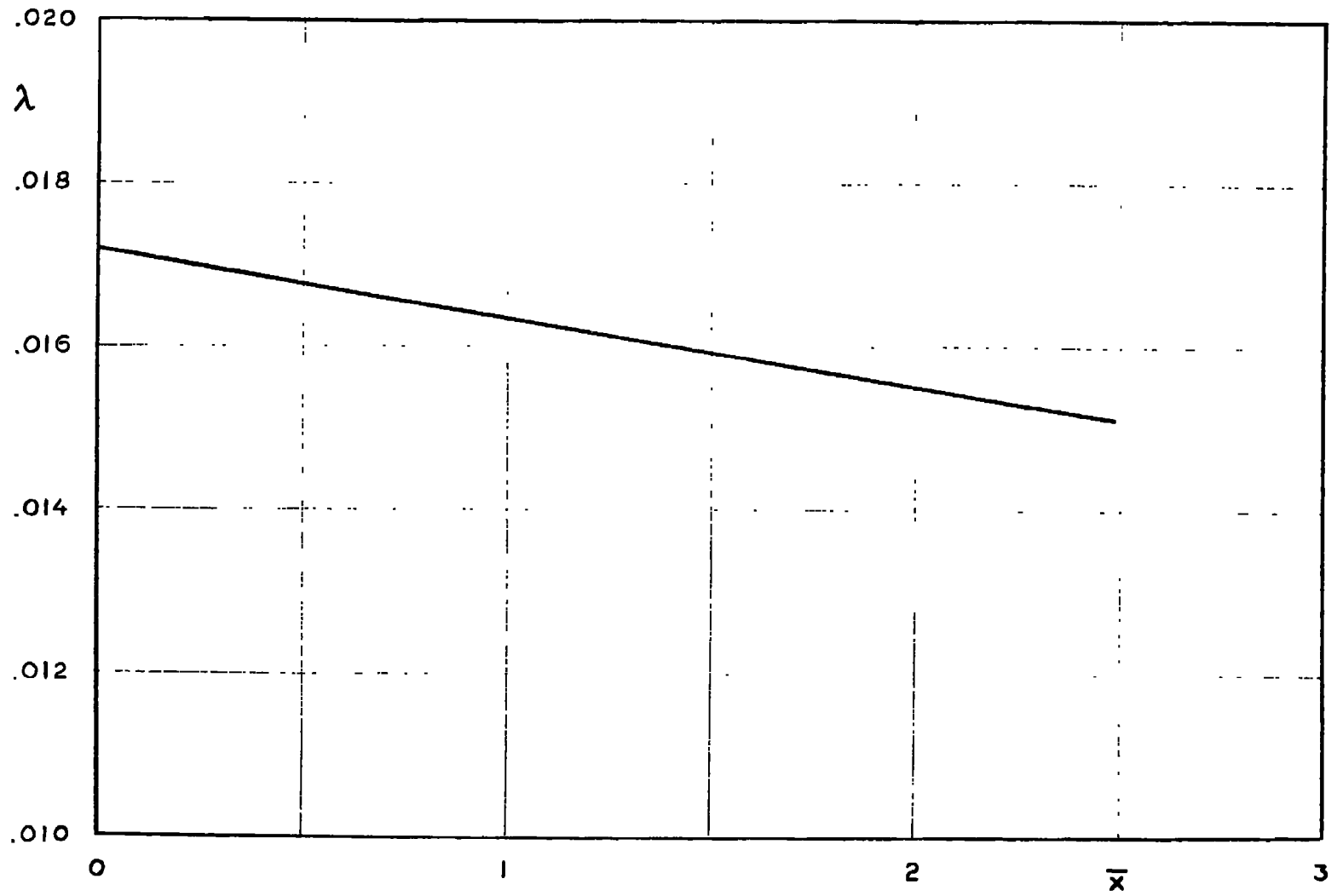
FIGURE 10.   PERIOD λ OF THE GRID IMAGE VERSUS $\overline{x}$

This particular case corresponds to the test grid with the center P_o located at

$$x_o = + 118 \text{ mm}, \quad y_o = -7 \text{ mm}, \quad z_o = 1,782 \text{ mm}$$

In the frame of reference of Figure (9) where the origin is placed on the plane of image. The angles ψ and θ defined in Equation (7) are

$$\phi \sim 45° \quad ; \quad \theta \sim 1°$$

The values of x_o, y_o, z_o were measured by triangulation from the two positions of the camera and the angular cooredinates were measured following the procedure outlined in SECTION III-2.

In Figure (10) one observes that for all practical purposes $\lambda(\bar{x})$ is a linear function of $\bar{x}$. This approximation is found to be valid in the total range of positions and orientations of the test grid and obviously it amplifies the computation of λ_i and $(d\lambda/d\bar{x})_i$. The value of λ_i can be assumed to be equal to the average value of λ over the number of lines of the grid image and $(d\lambda/d\bar{x})_i$ is the average derivative of the plotting of λ versus $\bar{x}$. In the image corresponding to Figure (10) one has

$$\lambda_i = 1.61.10^{-2} \text{ mm} \quad ; \quad \left(\frac{\partial \lambda}{\partial \bar{x}}\right)_i = 8.2.10^{-4}$$

As shown in SECTION III-3 the test grid position and orientation can be derived also from the above measured parameters of the grid image. The parameter v of the camera was measured at 35.54 mm in the initial calibration work conducted with the Xenon lens. By means of the set of equations developed in SECTION III-3 one can obtain the values of the coordinates of P_o and the angular coordinates of the grid. One has

$$x_o' = 116.6 \text{ mm}, \quad y_o' = -7.5 \text{ mm}, \quad z_o' = 1.755 \text{ mm}$$

$$\phi' = 43° \, 55' \, , \quad \theta' = + 1° \, 10'$$

(17)

Thus, the computed values of position and orientation are found to be fairly close to the values measured directly on the test grid. One observes, however, that the differences between the two measurements are larger than the specified precision of both translational and rotational distortions of the test surface. Consequently, the measurements of grid position and orientation extracted from the data of the images would not offer the required precision for measuring model distortions.

Apply now a rotation of the test grid about the vertical axis, i.e., the axis y in the frame of reference of Figure (9) and let us consider the two images corresponding to the rotations

$$\delta\phi \quad \pm \; 2°$$

while all other parameters of the test grid remain unchanged. The measured changes of the value of λ_i are

$$\delta\lambda_i \; \Big| \; \delta\phi = + \; 2° = .046.10^{-2} \text{mm}$$

$$\gamma\lambda \; \Big| \; \delta\phi = + \; 2° = -.049.10^{-2} \text{mm}$$

(18)

One can now use the set of parameters extracted from the measurement of the geometrical parameters of the image of the grid in the original position $(\delta\phi = 0)$.

With the aid of the equations developed in SECTION III-3 one obtains

$$\frac{\partial\lambda_i}{\partial\phi} = 2.35.10^{-4} \text{ mm/degree}$$

$$\frac{\partial}{\partial\phi}\left(\frac{\partial\lambda}{\partial x}\right) = 1.48 \times 10^{-5}$$

(19)

Then the values of the angular rotation of the grid corresponding to the set (18) of values of $\partial\lambda_i$ can be computed with the equations of SECTION III-4 and one has

$$\partial\phi = + \; 1° \; 57' \qquad \text{for} \qquad \partial\lambda_i = 4.6.10^{-4} \text{ mm}$$
$$\partial\phi = - \; 2° \; 8' \qquad \text{for} \qquad \partial\lambda_i - 4.9.10^{-4} \text{ mm}$$

which shows a very good agreement with the measured values of $\partial\phi$. A plotting of the values of λ measured in the three images corresponding to $\partial\phi = 0$, $\partial\phi = \pm 2°$ is shown in Figure (11).

A displacement of the test grid along the axis y of the plane of reference of Figure (9) alters neither λ_i nor $(\partial\lambda/\partial\bar{x})_i$ in the image, and the measurement of the displacement is obtained from the translation of the grid image center along the axis y. At the distance z_o' of the grid with coordinates given by (17) one has

$$\frac{\partial y_i}{\partial y_o} = 2.066 \ 10^{-2}$$

Assume now a displacement of the test grid in the plane $y = y_o'$ and in a direction perpendicular to the plane of the grid. At the position given by values (17), the equations developed in SECTION III-3 yield

$$\frac{\partial\lambda_i}{\partial z_o} = -.99 \cdot 10^{-5} \quad ; \quad \frac{\partial\lambda_i}{\partial x_o} = -.84 \cdot 10^{-5} \tag{20}$$

Within the specified range of displacements the change of λ_i is too small to be measured with sufficient accuracy. For this reason, the displacement of the test grid center is extracted from the measurement of the change in position of the center of the grid image. Consider, for example, the case where the test grid is moved in the direction perpendicular to its plane by 39 mm away from the camera. The displacement is then given by

$$\delta x_o = -27.1 \text{ mm} \quad ; \quad \delta y_o = 0 \quad ; \quad \delta z_o = -28.1 \text{ mm}$$

With the values of (20) of both derivatives of λ_i one observes that the effects of δx_o and δz_o on λ_i partially cancel each other. The actual measured change of λ_i is

$$\delta\lambda_i \sim .5 \ 10^{-4} \text{ mm}$$

Thus, as expected, the displacement of the center of the grid generates only a minor change of λ_i and its gradient along the axis of the grid image and the value of the displacement is extracted from the measurement of the change of the x_i, y_i coordinates. It is worthwhile pointing out that the measurement of the position of P_i in the image is performed within a fraction of the width of the line at P_i. Consequently, the displacement of P_o is computed also within a fraction of the width of the line of the test grid which is equal to .5 mm.
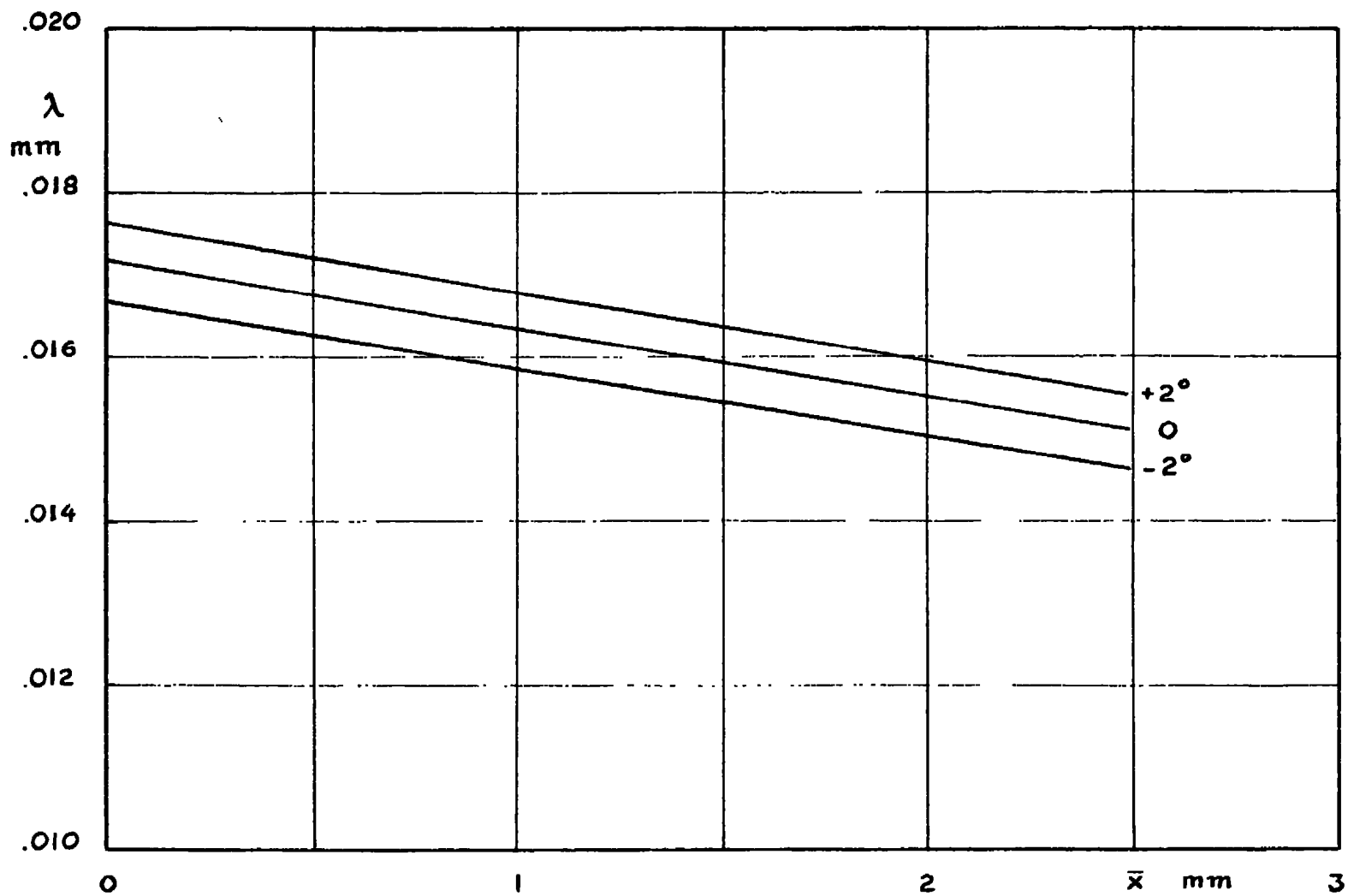
FIGURE 11.   PLOTTING OF λ VERSUS $\overline{x}$ FOR $\delta\phi = 0$, and $\delta\phi = \pm2^{\circ}$

Finally, it may be of interest to show the Moiré pattern generated by a direct superposition of two images taken with different positions or/and orientations of the test grid. Assume, for instance, the case of the grid with the center P_o located at

$$x_o = + 295 \text{ mm} \quad ; \quad y_o = - 7 \text{ mm} \quad ; \quad z_o = 1,662 \text{ mm}$$

and oriented according to the angles

$$\phi = 45° \qquad \theta = 1°$$

Apply a rotation $\delta\phi$ of the grid about the axis y in the frame of reference of Figure (9) and consider the images corresponding to $\delta\phi = + 2°$ and $\delta\phi = + 4°$ in addition to the image corresponding to the original position ($\delta\phi = 0$). Figure (12) shows the plotting of the position of the grid image lines in the three cases. The measured change in length of the grid images from $\delta\phi = 0$ to $\delta\phi + 2°$ is

$$\delta L_{2°} = .057 \text{ mm}$$

and the change in length from $\delta\phi = 0$ to $\delta\phi = + 4°$ is

$$\delta L_{4°} = .114 \text{ mm}$$

The average value of λ_i at $\delta\phi \ 0$ is

$$\lambda_i = 1.89 \ 10^{-2} \text{ mm}$$

Thus,

$$\delta L_{2°} \sim 3\lambda_i \quad ; \quad \delta L_{4°} \sim 6\lambda_i$$

i.e., the superposition of the two images $\delta\phi = 0$, $\delta\phi = + 2$ generates a Moiré with three fringes of the interference pattern and the superposition of the two images $\delta\phi = 0$, $\delta\phi = + 4°$ generates a Moiré with six fringes. The plottings of the interferences patterns computed from the measurement data of Figure (12) are shown in Figure (13). A Moiré pattern obtained with a double exposure of the test grid showing six fringes generated by a rotation of $4°$ is presented in Figure (14).
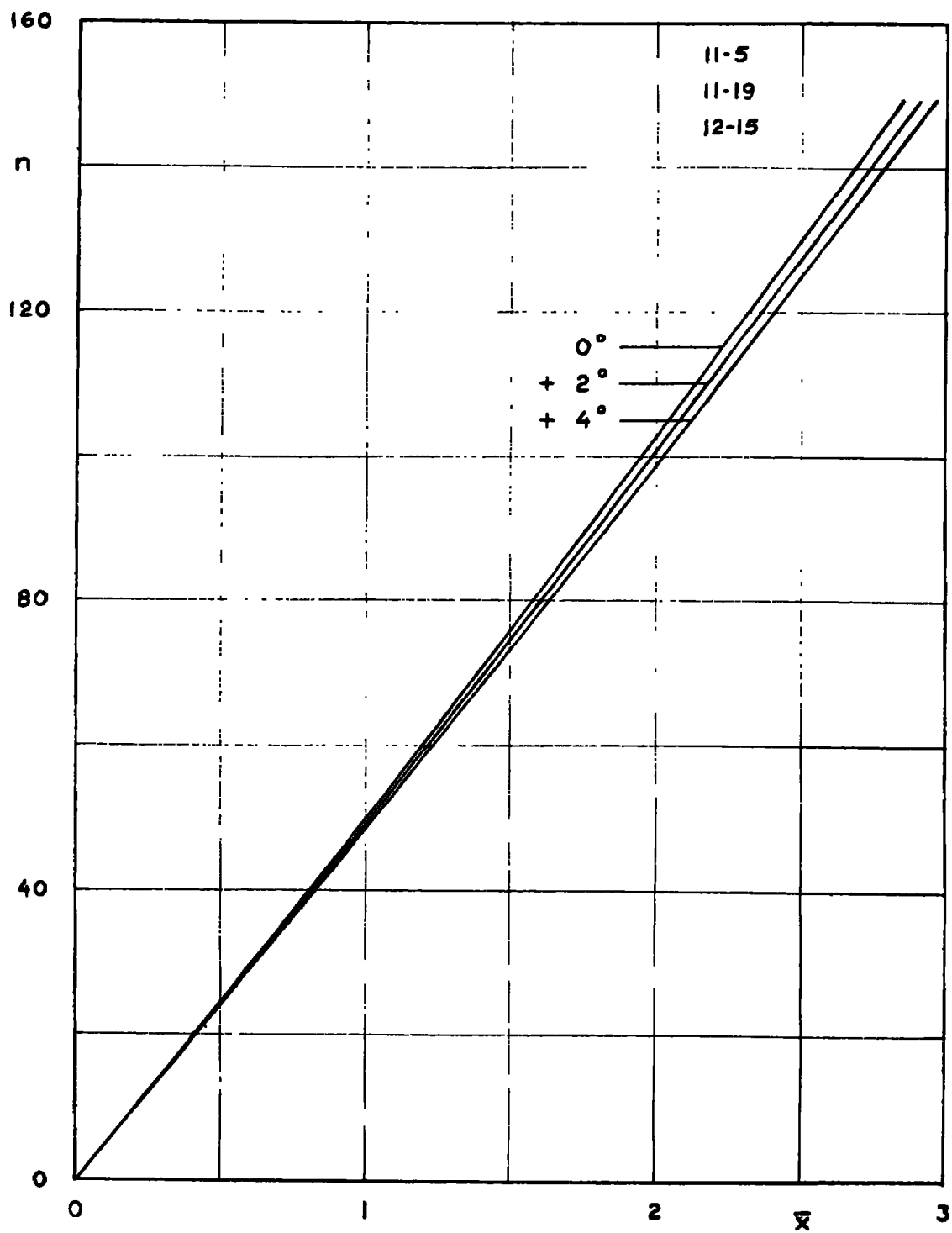
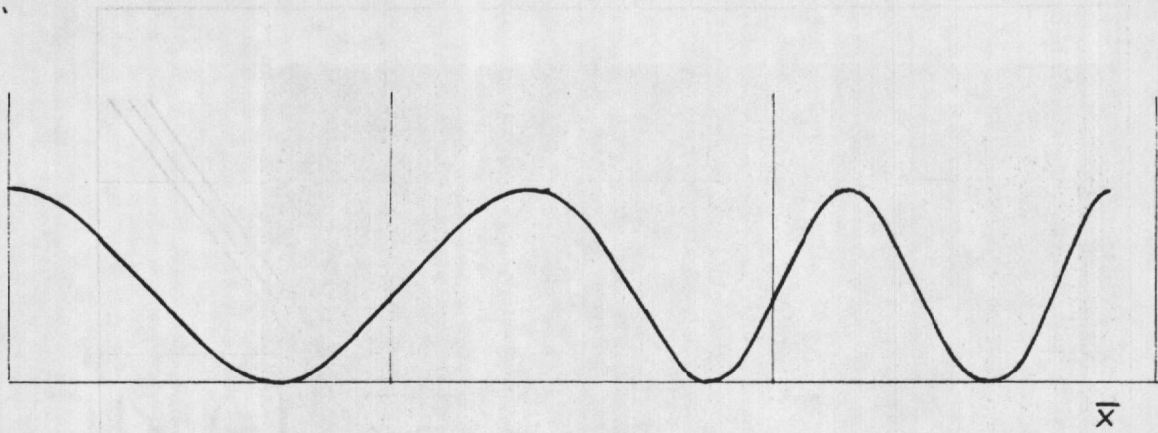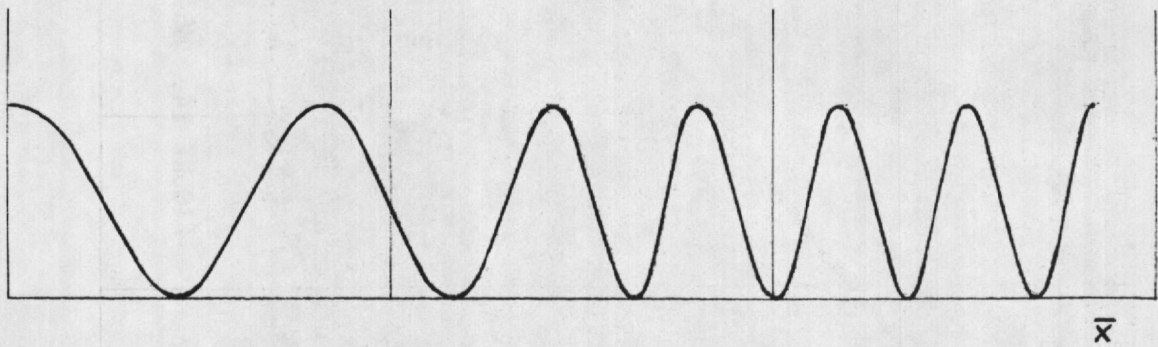FIGURE 12. POSITION OF GRID IMAGE LINES FOR THREE VALUES OF $\delta\phi$

FIGURE 13. INTERFERENCE PATTERNS CORRESPONDING TO SUPERIMPOSITION
OF IMAGES $\delta\phi = 0$, $\delta\phi = 2^{\circ}$ and $\delta\phi = 0$, $\delta\phi = 4^{\circ}$
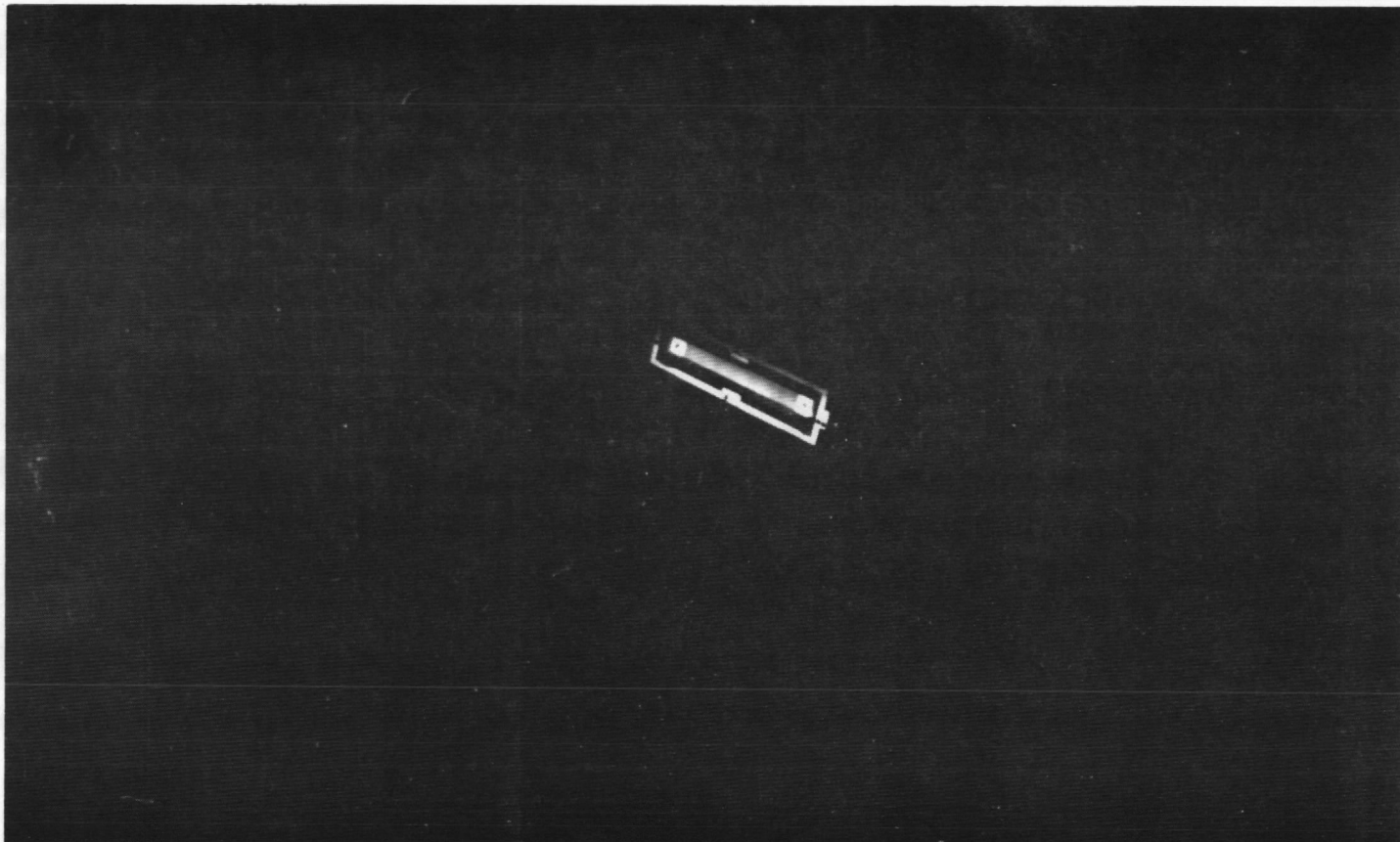
33

FIGURE 14. MOIRÉ PATTERN

As expected both λ_i and $(\partial\lambda/\partial\bar{x})_i$ vary substantially within the specified range of positions and orientations of the test grid. For instance, Figure (15) shows the length of the grid image versus the angular rotation about the axis $\bar{y}$ for the test grid oriented at

$$\phi = 45° \quad ; \quad \theta = 1°$$

and with the center P_o at

$$x_o = -4 \qquad x_o = 146 \qquad x_o = 295$$

$$y_o = -7 \qquad y_o = -7 \qquad y_o = -7 \qquad (21)$$

$$z_o = 1,958 \qquad z_o = 1,810 \qquad z_o = 1,662$$

Obviously, the length of the image increases as the distance z_o decreases. Figures (16) and (17) show the lengths of the grid images again versus the same angular rotation about the axis $\bar{y}$ for the same three positions of the center P_o given by (21) and the two angular orientations

$$\phi = 49° \qquad \phi = 60°$$

$$\theta = 30° \qquad \theta = 55°$$

One can observe that as ϕ and θ increase, the length of the grid image increases, however, the rate of change of the length of the image versus the angular rotation decreases. Obviously, the rate of change becomes zero for $\phi = 90°$, i.e., when the axis of the test grid is oriented perpendicular to the optical axis of the camera.

As previously mentioned the support of the test grid allows the simulation of the change of angle of attack in the HIRT facility. Figure (18) shows the dependence of the measured length L of the grid image versus the angular rotation about the axis $\bar{y}$ for 5 values of the angle of attack from $-10°$ to $+30°$. This figure corresponds to a grid inclined at 22° 30' with respect to the simulated axis of the test section of the facility. One observes that an increase of the angle of attack yields an increase of the length of the grid image and a decrease of the rate of change of L versus θ_y.

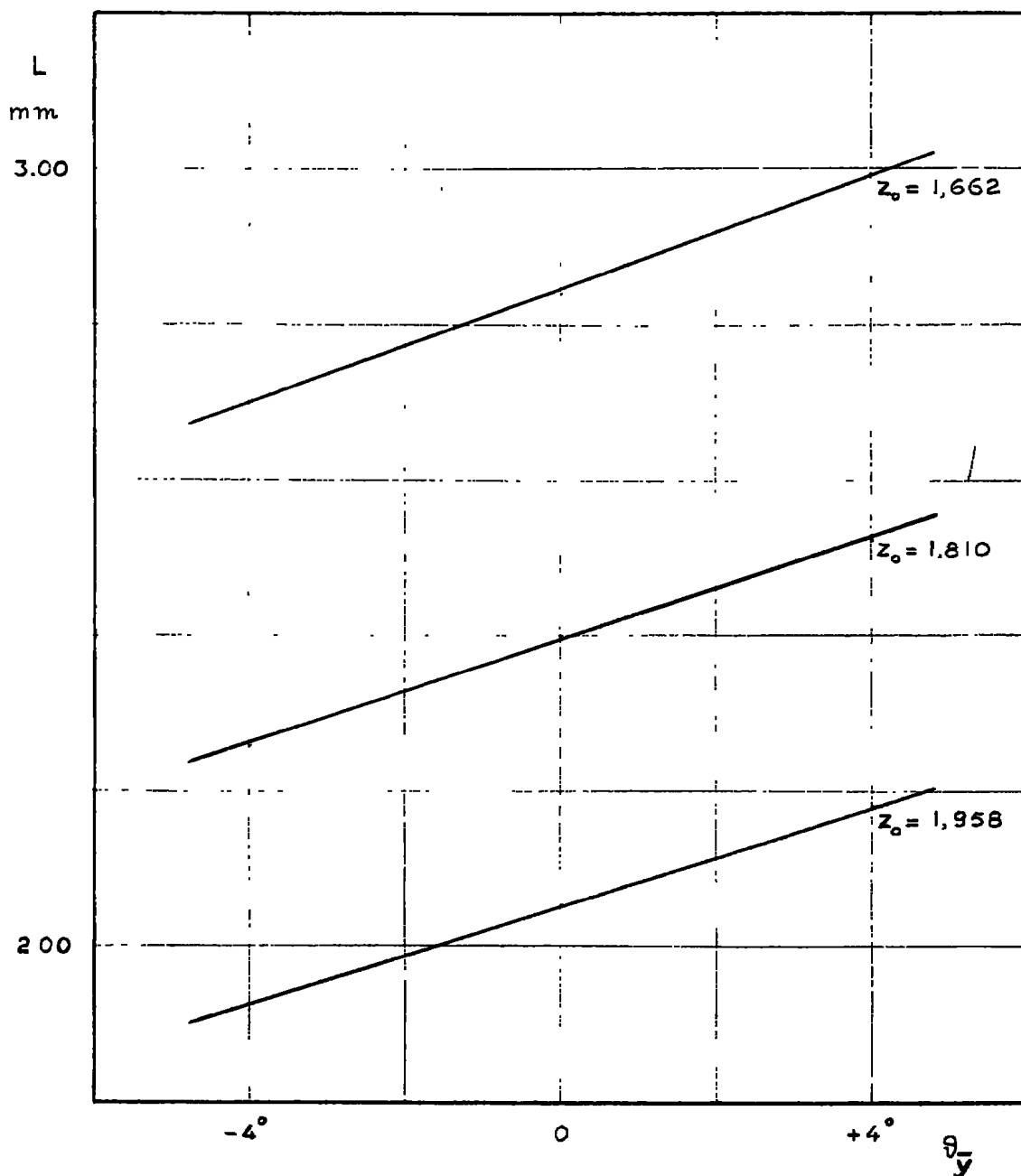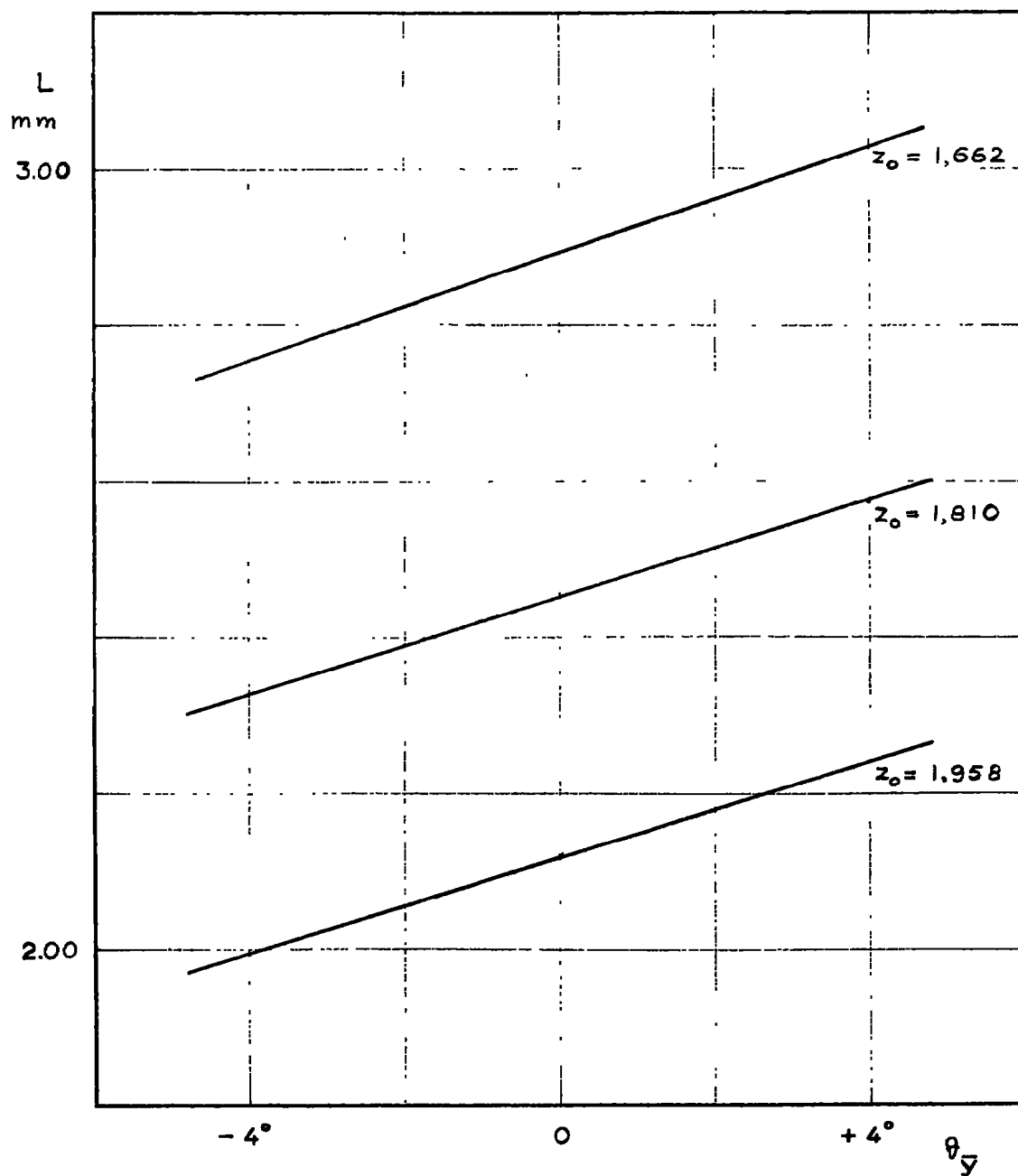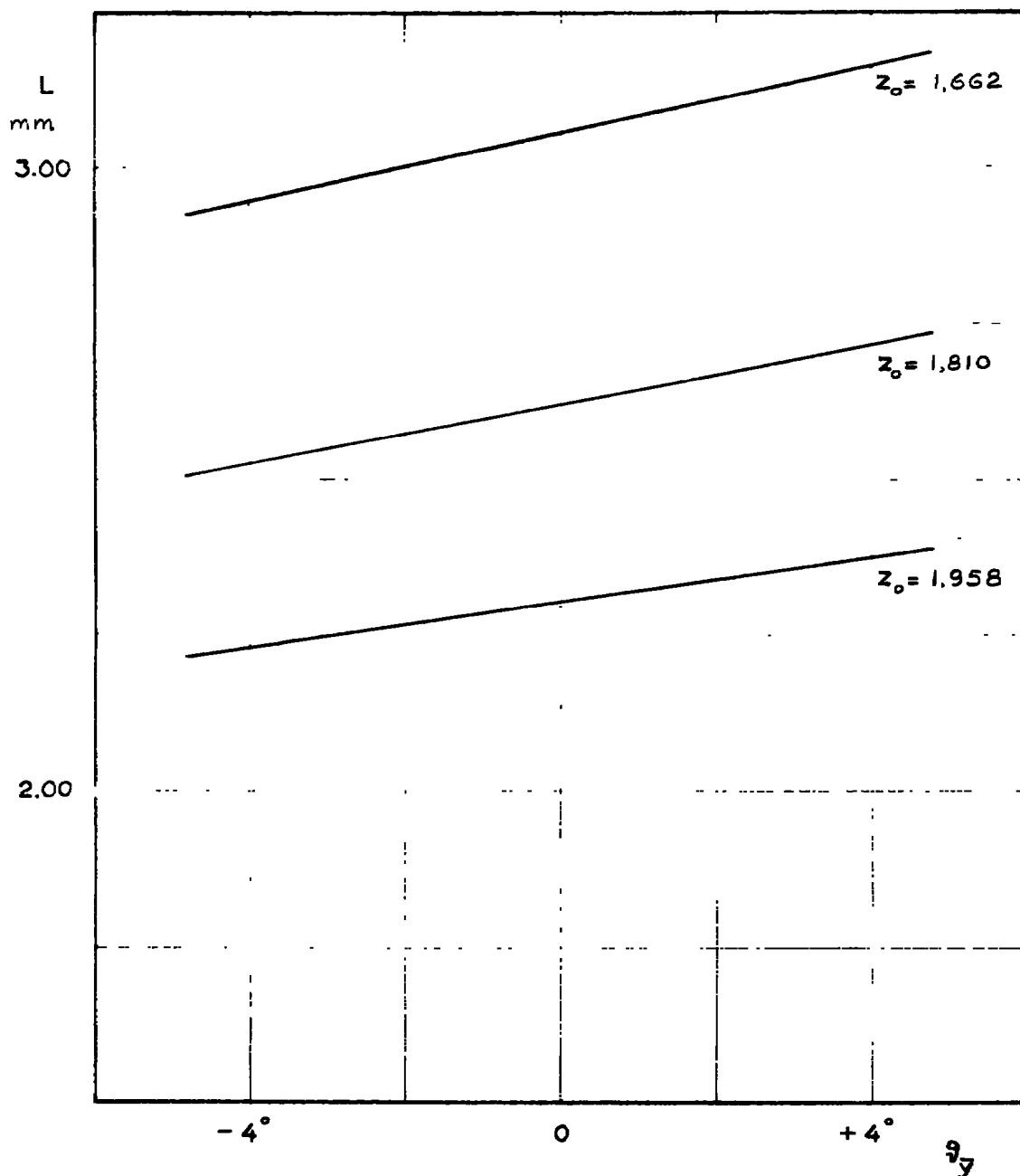FIGURE 15. EFFECT OF CHANGE OF GRID CENTER POSITION FOR $\phi = 45°$, $\theta - 1°$

.FIGURE 16.   EFFECT OF CHANGE OF GRID CENTER POSITION FOR $\phi = 49^\circ$, $\theta = 30^\circ$

FIGURE 17. EFFECT OF CHANGE OF GRID CENTER POSITION FOR $\phi = 60^d$, $\theta = 55^o$
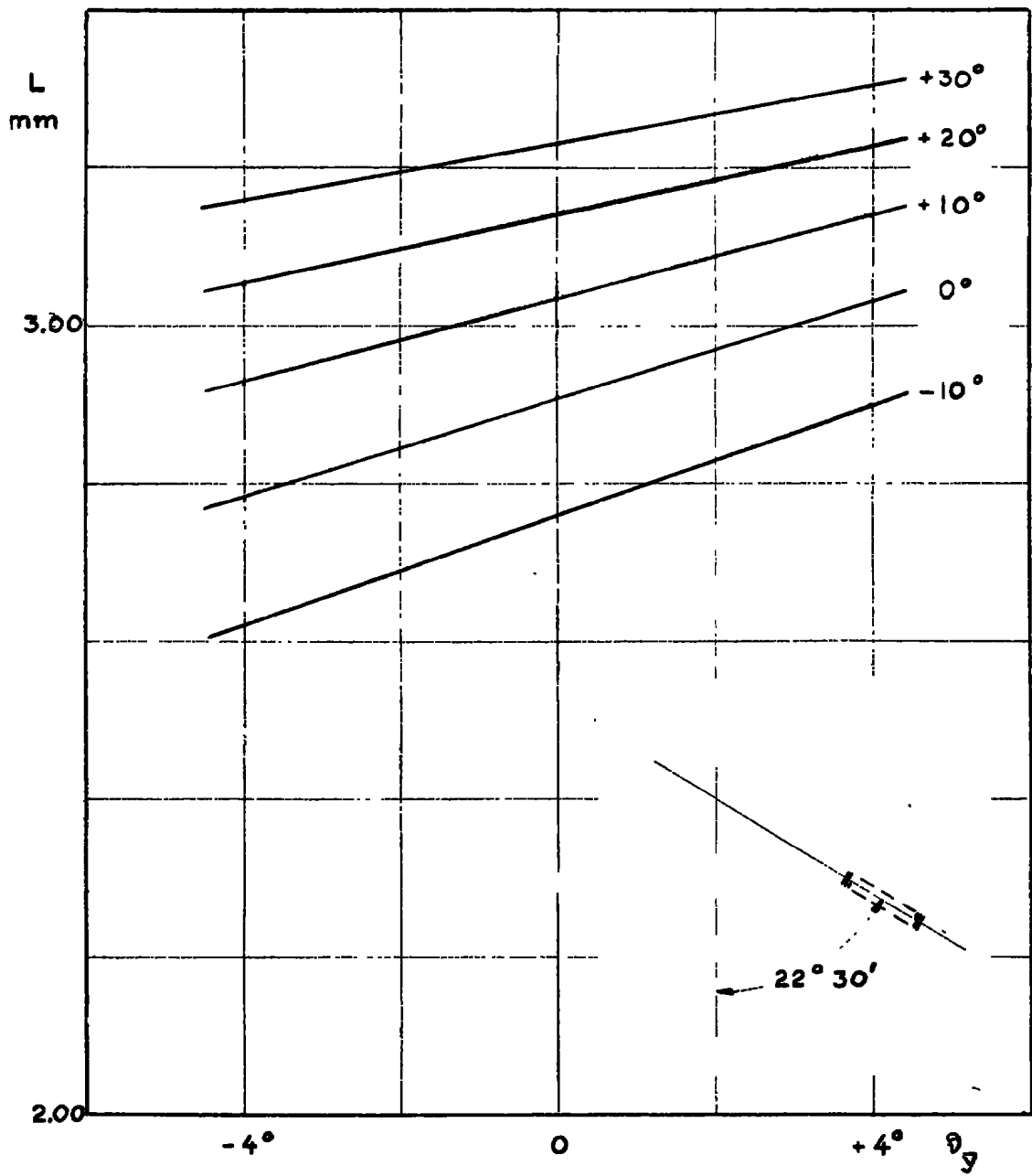
FIGURE 18.   EFFECT OF ANGLE OF ATTACK FOR AN ANGLE OF 22° 30'
BETWEEN GRID AXIS AND TEST SECTION AXIS

A comparison of the results obtained from the grid images with the direct measurements of the grid displacements and rotations is illustrated in Figure (19). The orientation of the test grid in this figure simulates a model of a wing swept back at 22° 30'. The rotation θ_y of the test grid simulates then the angular deflections obtained from the grid images versus the angular deflections measured directly in the grid support for the range of angles of attack from -10° to +30°. Over the total range, the precision of the measurement is maintained within .2 degrees.

FIGURE 19. VALUES OF $\theta_{z'm}$ MEASURED FROM THE GRID IMAGES vs THE VALUES OF $\theta_{z'}$ MEASURED DIRECTLY FOR DIFFERENT ANGLES OF ATTACK

SECTION IV

PROPOSED INSTRUMENTATION

4.1 INTRODUCTION

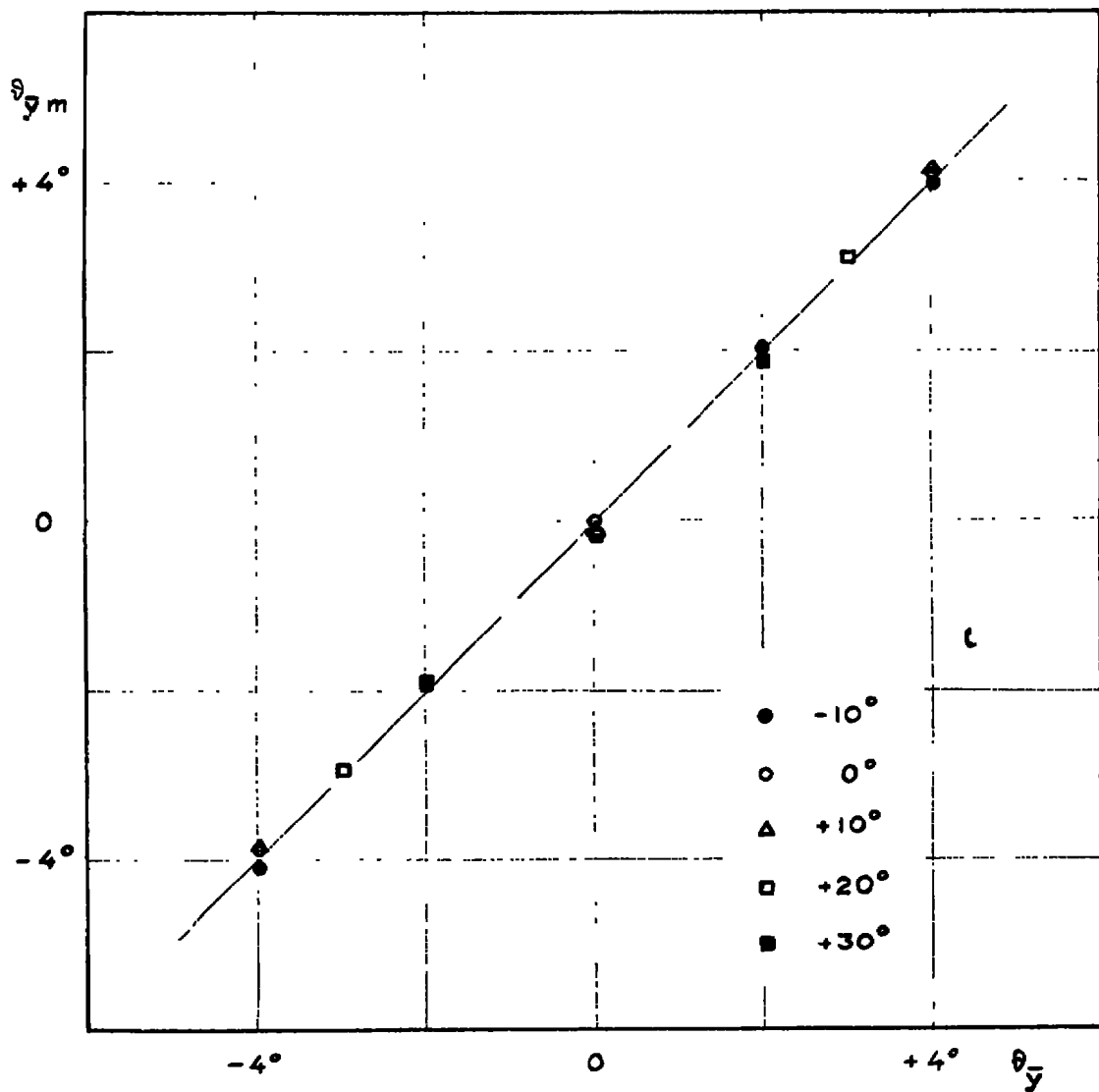The results obtained in the work described in the two preceding chapters can now be used to establish the basic criteria for selecting the suitable type of instrumentation and its components. The complete instrument would be formed by two major parts:

- Camera System

- Image Analyzing System

The camera system includes the two cameras which are going to be used to obtain the images of the test model prior to and during the test and the interfacing of the camera with the test section. Structural as well as aerodynamic problems pose rather severe constraints in the way the cameras can be mounted in the facility. The arrangement discussed in this section appears to provide a suitable solution which minimizes the flow perturbation. Furthermore, the 35 mm format allows the selection of compact cameras which should simplify the problem of integrating the camera system into the test section area of the facility.

As discussed in SECTION II, the type of film selected for this particular application is specifically designed for an automated rapid developing process. Once developed the films of the test surface are transferred to the image analyzing system to obtain the value of the local distortions. The image analyzing system involves a sequence of processes which may be grouped in two basic steps. First, the geometrical parameters of each grid image defined in the previous section must be measured in each frame of the film and stored. Second, these measurements are fed to a computer which compares the data obtained with the two cameras prior to the test and computes the geometry and position of the undistorted test surface. Subsequently the computer compares the data obtained with one of the two cameras prior and during the test and computes the values of the test surface distortion.

As discussed in SECTION III, only algebraic operations are involved in the process of estimating the distortion values from the pertinent parameters measured in the grid images. Consequently, no difficulty arises in the computational process. However, the complexity of the image analyzing system arises exactly in the measurement of the grid images. It is apparent that, in view of the large number of images obtained with the two cameras in each test, a fully automated system is required to perform the measurements of the pertinent parameters of the grid images in a reasonably short time. Thus the automated measuring process is the most critical step of the entire system because it controls the precision of the measurements and basically determines the time required to make the results of the experiment available after the test.

As discussed in SECTION III only algebraic operations are involved in the process of estimating the distortion values from the pertinent parameters measured in the grid images. Consequently no difficulty arises in the computational process. However, the complexity of the image analyzing system arises exactly in the measurement of the grid images. It is apparent that, in view of the large number of images obtained with the two cameras in each test, a fully automated system is required to perform the measurements of the pertinent parameters of the grid images in a reasonably short time. Thus the automated measuring process is the most critical step of the entire system because it controls the precision of the measurements and basically determines the time required to make the results of the experiment available after the test.

In the following sections first the camera arrangement is discussed and second the analysis of the various phases of the image processing system is presented. The basic criteria are given for the selection of the components of the final measuring system.

4.2 CAMERA ARRANGEMENT

The primary criteria for mounting the cameras in the HIRT facility is that no window in the wall of the test section may be larger than six inches in diameter. In addition, the number of windows should be kept to the minimum required for the two cameras and the lighting system.

A camera particularly suitable for the application in the Photo-Sonics high speed camera model 33 mm - 4M. The camera is electrically driven with a frame rate electronically controlled to $\pm$ 1%. A 180 fps speed is currently available. The film transport mechanism is intermittant with four pulldown pins and two register pins. This insures steady images during the camera run. The camera accepts three interchangeable magazines with film capacities of 200, 400 and 1,000 feet. The 200 foot magazine would be selected to record the 2.5 secs of run time of the facility at the speed of 180 fps and this results in a compact camera body. The camera dimensions are shown in Figure (20).

A ground glass viewfinder is provided as a unit which is interchangeable with the film magazine for alignment and focussing of the camera before the test. The commercially available viewfinder is intended for a conventional use of the camera and may not be suitable for this specific application where the camera is mounted in a confined space within the outside wall of the facility. The optics of the viewfinder may then have to be modified to bring the image at a position convenient for the operator.
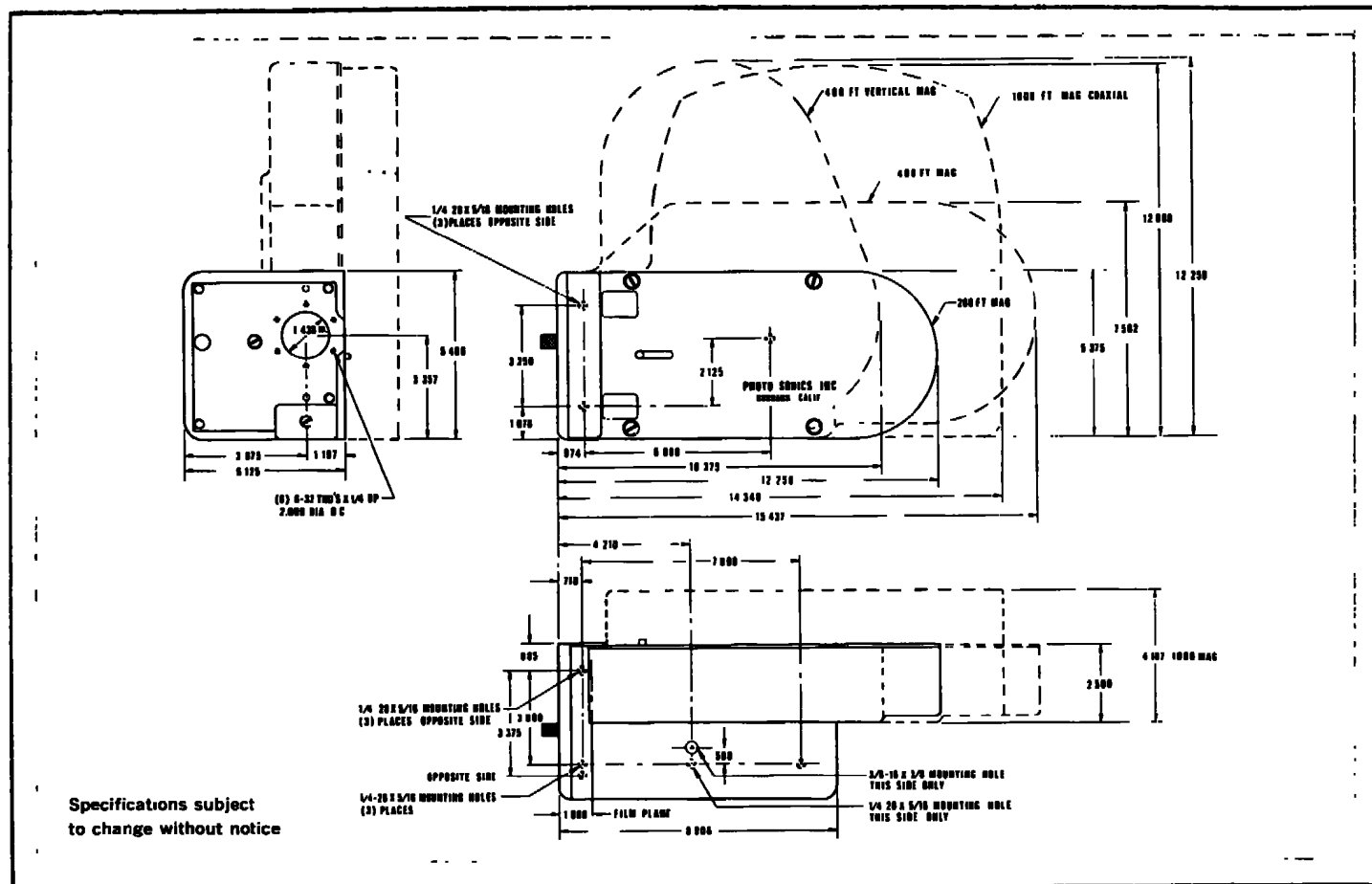
Specifications subject
to change without notice

FIGURE 20.   PHOTO-SONICS CAMERA DIMENSIONS

Each camera would be equipped with the Schneider Kreuznach Xenon 1:2/35 lens
and the same optical arrangement used in the data collection of the present
would could be adapted to the final camera assembly. As shown in Figure (21)
a beam splitter would be positioned in front of the lens to provide the
image of a matrix of refernece points mounted on the same support of the
camera.

Mounting holes are provided on the top, bottom and right side of the camera
thereby presenting a sturdy mounting of the camera on its supporting structure.
Each camera would be mounted in a hermetically sealed compartment for its
protecting in the facility environment, as indicated in the schematic of
Figure (21). The compartment would be provided with a window flush with the
inner wall of the test section and could house all the necessary electrical
and mechanical connections for the remote control of the camera. The compart-
ment would be attached by a supporting frame with provisions for removing it
in order to change the film magazine and service the camera.

4.3 SCANNING AND DIGITIZING OF THE IMAGES

The first step of the automated measurement of the geometrical parameters of
the grid images is an electronic scanning of the frames of the film. The
output of the scanner is then digitized and processed into a format suitable
for input to a data reduction software package.

Automated precision scanners are commercially available; however, due to the
minimum spot size which can be achieved with a vidicon scanner, it is impossible
to scan in one step the entire area of the frame with the resolution required
for accurate measurement of the grid parameters. A typical scanner has a scan
standard of 720 lines, with no interlace, and each line is divided in 890
separately resolvable points. This corresponds to a matrix of approximately
30 separately resolvable points for millimeter of the frame of the film.
As shown in the previous section a typical grid image contains approximately
50 lines per millimeter. Thus, to achieve the required resolution a magnifi-
cation from one to two orders of magnitude is required in the projection of
the grid images on the screen of the vidicon. As a consequence grid images
distributed over a large area of the film frame must be scanned independently
and, also the image of the 150 line grid, like the one used in this program
may have to be scanned in two separate steps.

Based on these considerations the following functions must be performed in the
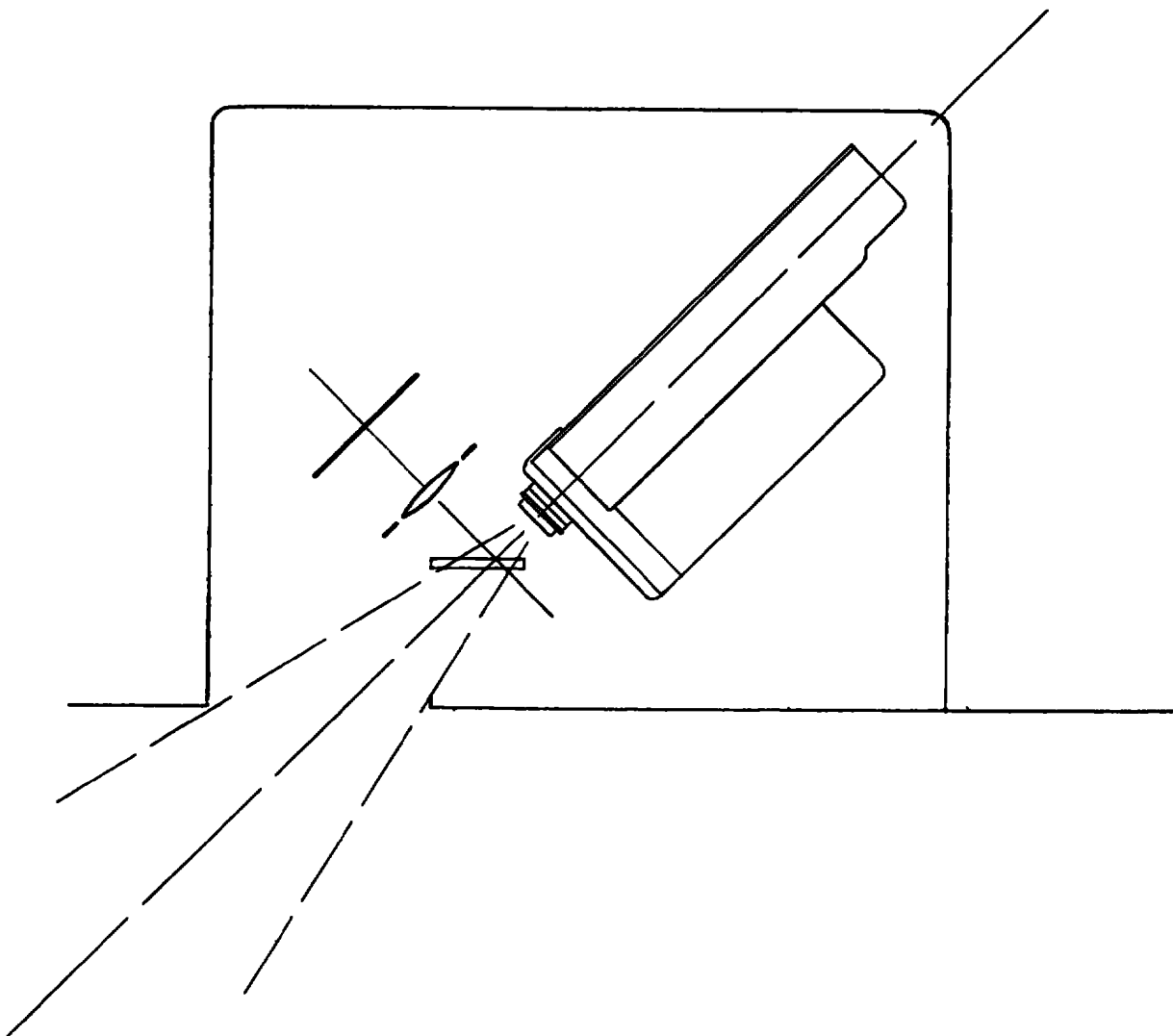automated scanning process:

FIGURE 21.   SCHEMATIC OF CAMERA ARRANGEMENT

(a) Scan the full area of the individual frame
to locate each grid image

(b) Magnify the frame and bring the image of each
grid, or fraction of grid, into the field of view
of the vidicon scanner

(c) Scan each grid image and measure the geometrical
parameters of the grid images, including the
relative position and orientation of the various
grids

Automated scanners are available which can be programmed to select a predeter-
mined position of the frame. However, they are not directly applicable to
this particular problem because the total area of the grid images is a relative-
ly small fraction of the frame area and, in addition, the position of each grid
image may shift substantially in a film due to the changes of model pitch during
the test. It must be kept in mind that a typical .5 secs dwelling time of the
film frame in front of the scanner lens is required before the scanning of the
frame may start. This time must be added to the time required to mechanically
move and lock the frame in front of the scanner. Thus by subdividing the frame
in a matrix of adjacent areas, and by scanning independently each area in order
to locate each grid image, an intolerable amount of time would be spent in the
image processing.

It appears then that the best approach which minimizes the scanning time is a
combination of low magnification scanning which locates each grid image and
provides a coarse measurement of its position, followed by a high magnification
scanning which accurately measures the parameters of each grid image. The
position of the frame during the high magnification scanning would be controlled
by the output of the low magnification measurement.

The scanning process could then be accomplished by using two independent scanners:
a first scanner whose magnification is such that the entire frame is contained
within the field of view of the vidicon, followed by a high magnification
scanner with a programmable stage controlled by a mini-computer module to scan
the individual grid images. Apart from the complexity of the independent
scanners the main disadvantage of this approach is that a film frame has to
move from the first to the second scanner over a minimum distance of the order
of 10 to 20 frames.

A second solution would make use of a single scanner with a programmable stage
equipped with two optics; a low magnification optics covering the entire frame
which would be automatically replaced by a high magnification optics for the
scanning of the individual grid images. This second solution appears to pro-
vide the most appropriate approach. The scanning system would then be built
according to the schematic of Figure (22) and the entire process would proceed
as follows:

(a) A film transport mechanism advances the 35 mm film and locks a frame on a programmable stage into the field of view of the low magnification lens of the scanner. The stage is controlled in such a way that the center of the frame is positioned on the axis of the optical system and the entire frame is contained within the field of view of the vidicon tube.

(b) After a .5 secs dwelling time of the frame in front of the lens, the frame is scanned. A typical scanning time figure is 100 ms. In this first operation the magnification of the lens is too low to resolve the lines of the grid images and only the gross features of each grid image can be detected. For instance, the position of the left hand side corner of each grid image in the frame is identified by the scanner and the corresponding coordinates are stored in the memory of a mini-computer module. The maximum error in measuring and digitizing these reference points would be of the order of 10 line spacings.

(c) The low magnification lens of the scanner is replaced by the high magnification lens. The time required to mechanically switch the optics of the scanner is estimated at about 1 sec or lower.

(d) As the optics of the scanner is being switched, the output of the mini-computer module provides the signal which controls the position of the programmable stage and the frame is moved in such a way as to place one of the grids reference points within the field of view of the high magnification lens. The projected time for altering the position of the programmable stage from one reference point to the next is about 1 sec or lower. Thus the locking of the stage at the first reference point would occur during the interval of time required to switch the optics of the scanner.

(e) After a dwelling time of .5 secs, the image of the grid (or fraction thereof) is scanned in approximately 100 ms. The output of the high magnification scanning is fed to a calculator which extracts the required digital data, i.e., poisition of the grid image reference point, orientation of the grid image axis and distribution of line spacings along the grid image axis.

(f) Upon completion of the scanning of the first grid image, the programmable stage brings the reference point of the second grid image within the field of the view of the scanner, and the process of scanning and digitizing is repeated. The entire procedure is then repeated for all the grid images contained in the frame. Assuming for instance a total number of six grids per frame and a scanning of each grid in two sections, the total time required to scan and digitize each frame of the film would be approximately 21 secs. Thus with a 2.5 sec run time and a camera speed of 180 frames per second, the scanning and digitizing of all the frames of the film would be performed in approximately 2.5 hours.

(g) Upon completion of the high magnification scanning, the following frame is moved into the programmable stage which again positions the center of the frame on the optical axis and at the same time, the optics of the scanner is switched back to the low magnification lens. The entire scanning procedure of the new frame is then repeated.

In this approach the programmable stage has only the two translational degrees of freedom which correspond to the x, y axes of the film frame. Thus the angle between the axis of the grid image and the axis x of the reference system would be extracted from the measured values of the x, y coordinates of the center points of each line of the grid image.

A critical point of the high magnification scanning and digitizing process is how the reference system of x, y coordinates can be established with the required precision for each portion of a frame and for the entire sequence of frames of the film. It is apparent that the positioning of the reference point of the first grid image in front of the high magnification lens is performed with a precision limited by the resolution of the low magnification scanning process. In principle this would be of no consequence since in each frame only the relative position of the various grid images is of importance. The problem could then be solved by controlling the x, y position of the programmable stage with a precision consistent with the resolution of the high magnification scanning. In this procedure, each time the programmable stage is moved to scan another portion of the film frame, its position has to be measured with high precision and the measurement must be added to the output of the high magnification scanning, in order to obtain the exact position and orientation of the grid images relative to each other. It follows that if the relative position of each grid image has to be determined within a fraction of the line spacing (say, for instance one tenth of the line spacing) a precision better than 2μ is required in the mechanical control and measurement of the position of the programmable stage.

A simpler solution which does not require the high precision control of the stage and eliminates the associated mechanical and electronic problems, is offered by superimposing the images of reference points on the film frame at the same time that the images of the grids are taken. This can be accomplished as shown in Figure (21) where a beam splitter is used to superimpose the image of a matrix of reference points on the frame of the film.

Within the expected range of distortions of a test model the maximum displacement and rotation of each grid image in a frame of the film should be within the dimensions of the grid image itself. Thus, the matrix of reference points should have a period of the reference point of the same order of the dimensions of the grid image. A variety of geometrical shapes of the matrix reference points could be selected. The most convenient shape appears to be a circular dot, which has the advantage over other shapes of simplifying the problem of locating the center of the dot in the scanning process. The reason is that as the scanning spot of the scanner moves on a horizontal line tangent to the circular dot image, the position of the center of the dot is automatically determined by either adding or subtracting to the vertical coordinate of the line the known value of the dot radius. This is true regardless of the orientation of the film frame on the programmable stage. Consequently, the superimposition of such a matrix on the film frames not only provides the frame of reference of the grid images, but also eliminates the need of an extremely accurate registation of the film on the stage.

A problem of ambiguity in identifying the same reference point in two different frames of the film could arise if there is a substantial change in position of the grid image. This problem is easily eliminated by a simple coding of the reference points like, for instance, by selecting different diameters of the reference dots at alternate points of the matrix. Figure (23) shows an example of such a method obtained beam splitter arrangement.

The schematic of Figure (22) presents the basic system components required to implement the measuring and digitizing process. The system is composed of two major groups: the 35 mm Cinescan and the Image Analyzer.

The 35 mm Cinescan would be fitted with a high speed forward and reverse flux transport mechanism and single frame automatic stopping. In addition, this unit would move the programmable stage to properly position each grating image within the field of view of the high magnification lens. The input to the controller of the transport mechanism is provided by the programmer unit of the Image Analyzer and the input for the position control of each frame is provided by the mini-computer. Figure (22) shows the two lenses on the lens turret, one to image the full 35 mm frame and the second, with approximately 30 magnification, to image each of the grids. The selection of the lens turret position is made with a controller unit whose input is provided by a programmer unit of the Image Analyzer.
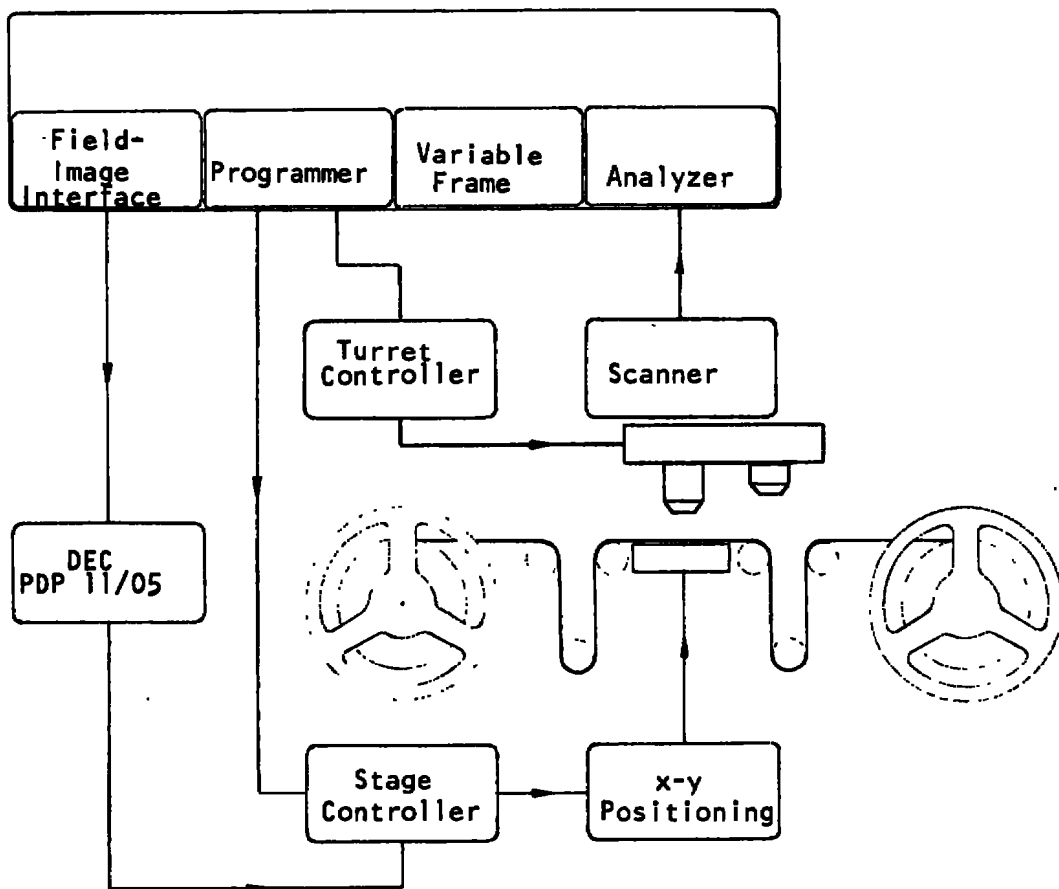
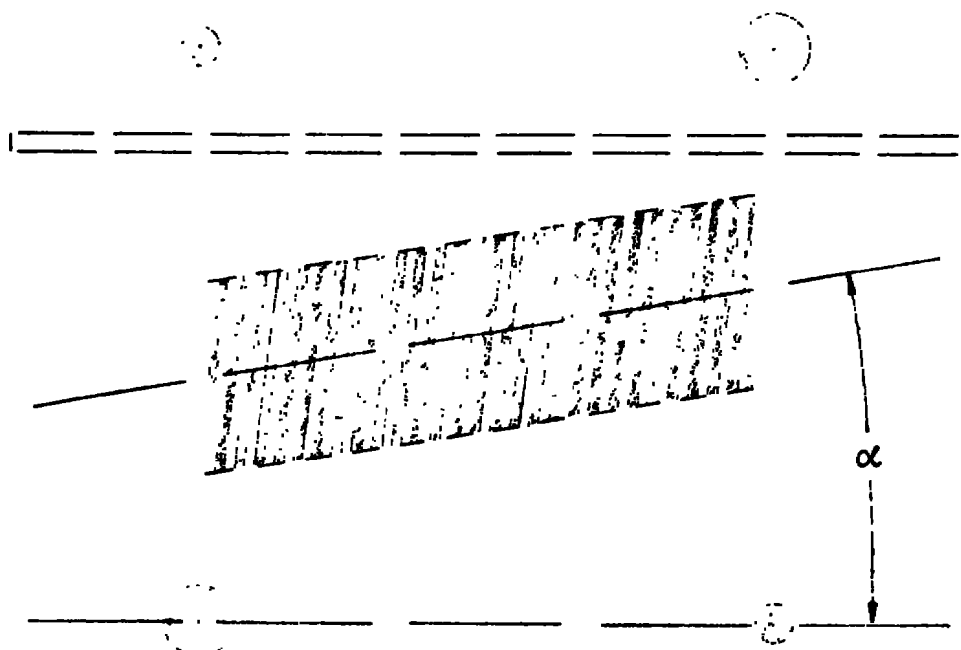FIGURE 22. SCHEMATIC OF THE SCANNING SYSTEM

FIGURE 23. GRID IMAGE WITH REFERENCE POINTS

The electronic scanning of each image is controlled by the Image Analyzer Programmer. The scanning line is oriented along the x-axis and moves in the y-direction as shown schematically in Figure (23). Thus, the position of each line of the image is obtained by the measurement of the position of both upper and lower points of contact of the grid line with the scanning line. Also, the positions of the points of contact of the reference circular dots with the scanning line is measured. The separation between data of the grid lines and data of the reference points is automatically achieved with a pattern recognition module which makes use of the value of the ratio of area to the square of the perimeter of both images.

The x, y data of the grid lines and reference points are fed to the mini-computer by means of an interface unit of the Image Analyzer. The slope of the grid image, i.e., the angle α of the grid axis with respect to the x axis is obtained from the coordinates of the contact points of the scanning lines with the grid lines. The computer then compares the spacing of the grid lines along the grid image axis, from which both average values λ_i and $(d\lambda/d\aleph)_i$ are obtained. Also the positions of the centers of the reference dots are computed from the coordinates of the points of contact of the dots with the scanning line. All these data are stored on magnetic tape for subsequent calculations of grid position prior to the test and grid displacement during the test. In addition, the mini-computer provides the position of the grid images to the controller of the programmable stage to properly locate the high magnification field.

The 35 mm Cinescan is a special unit which would be built for this specific application. A commercial high precision Cinescan would be modified to include the electro-mechanical controls of the lens turret and the stage position. The components of the Image Analyzer are commercially available with the exception of the interface module to feed the analyzer output to the minicomputer. A typical analyzer, capable of performing the afore-mentioned function is the Quantimet 720 manufactured by Image Analyzing Computers, Inc. A mini-computer which could be used in the approach of Figure (22) is the DEC PDP 11/05, including DEC Cassette, DEC Writer, DR 11B Interface Card, CAPS II Software and 16 K Core.

A test of the automated scanning process was performed in the Quantimet 720 system, using commercially available modules of the system, and by manually controlling the film frame position on the microscope stage. The purpose of this test was to verify the validity of the approach described in this section and, in particular, to determine the optimum image magnification of the scanner required to achieve the desired resolution.

Figure (24) shows the image of a test grid observed on the video monitor of the Quantimet 720 System. Figure (24a) presents the image of the test grid alone, and in Figure (24b) superimposed to the grid image is the variable frame which moves vertically through the image to perform the electronic scanning. Figure (25) shows a fraction of the grid image obtained with high magnification of the scanner. The number shown on the right hand side of the video screen is the location of the scanning variable frame and the number shown on the left hand side is the number of lines of the grid image contained within the variable frame which are automatically counted by the analyzer module of the Quantimet system.
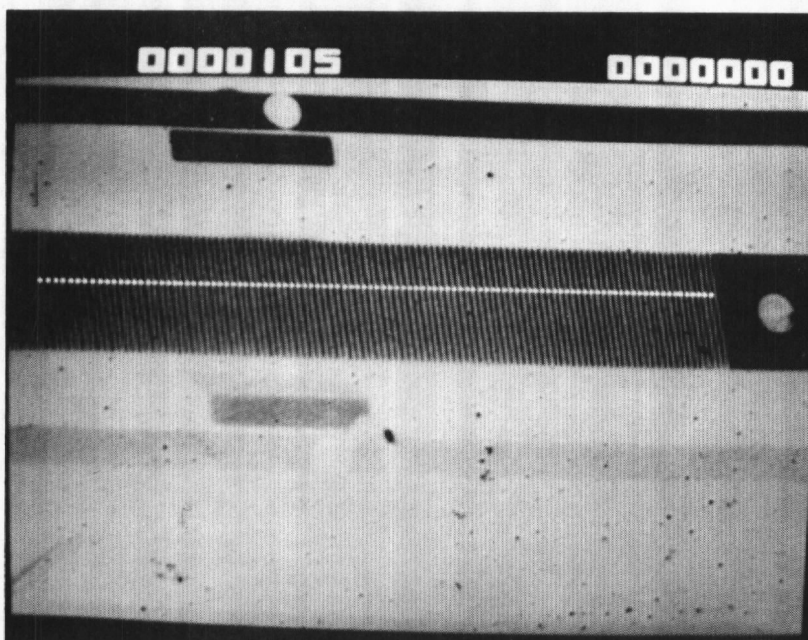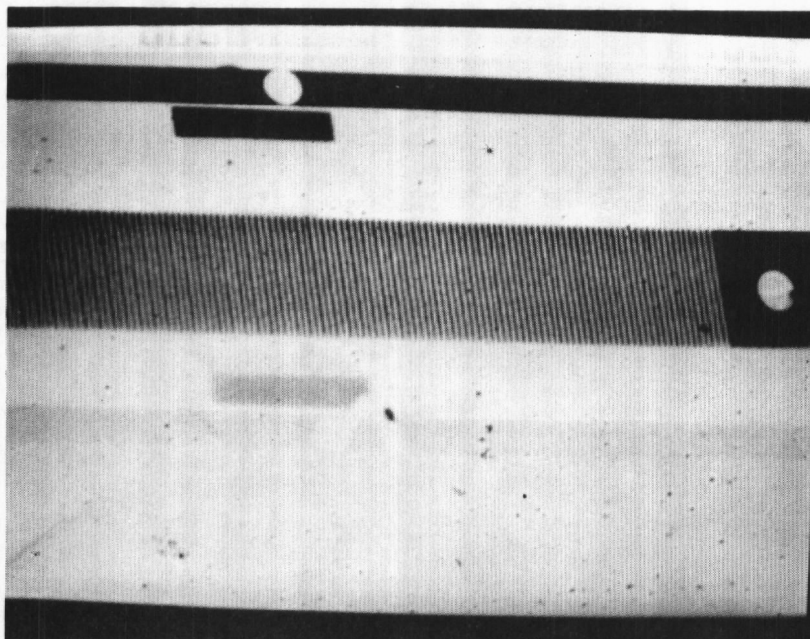
FIGURE 24. GRID IMAGE OBSERVED ON THE SCREEN OF THE
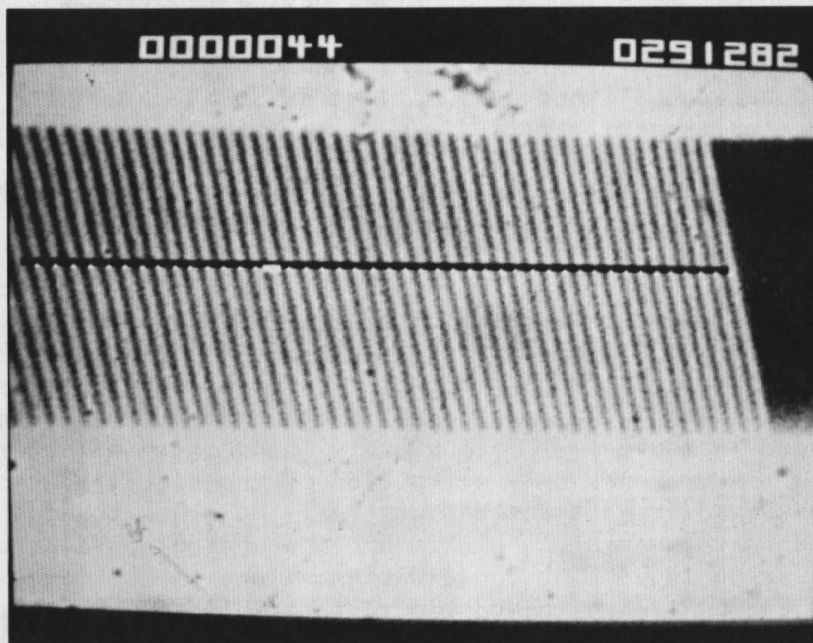VIDEO MONITOR OF THE QUANTIMET 720 SCANNER

FIGURE 25. ENLARGED IMAGE OBSERVED ON THE VIDEO MONITOR

4.4 CONCLUSIONS

The results presented in Chapter 3 show that the specified resolution and precision are achieved with the recommended format of the camera system and with available commercial film. Both the optical arrangement and the electronic scanning system described in this chapter appear to provide the simplest approach to the automated analysis of the images obtained in the specified experimental conditions of the HIRT facility. All the basic components of the camera, and scanning and digitizing system are available, with the exception of the electro-mechanical device required to switch the image scanning process from the preliminary low magnification phase to the high magnification, high precision, phase. The construction of the switching device would be accomplished by modifying existing components to adapt them to this particular application.

The precision achieved in the measurements performed during the present program is consistent with the maximum resolution attainable with the recommended format and film. It follows then that an increase in the precision of the measuring system could be achieved if the field of view of the camera were limited to a fraction of the dimensions specified for the present program. By increasing the focal length of the camera lens, the number of lines per millimeter of the grid image decreases and consequently the precision of the measurement of the geometrical parameters of the grid images increases. This obviously means that to increase the precision of the measurements only a fraction of the specified test surface area could be observed at each instant of time. No other changes would then be required in the measuring system and the photographic data would be collected by substituting a long focal distance lens to the one used in the present program and by aiming the camera to the region of the test surface where the measurements have to be performed.

REFERENCE

1. Abele, M., Ruger, C. and Sanlorenzo, E. "Study of Moiré Measuring Techniques for Wind Tunnel Model Deformation." AEDC-TR-73-154 (AD766892), March 1973.